The Thesis Committee for Faik Ozcan Polat
Certifies that this is the approved version of the following thesis:

Core-Seismic Correlation and Sequence Stratigraphy at IODP Expedition 317 Drillsites, Canterbury Basin, New Zealand

APPROVED BY
SUPERVISING COMMITTEE:

Supervisor:

Craig S. Fulthorpe

William L. Fisher

Ronald J. Steel

Core-Seismic Correlation and Sequence Stratigraphy at IODP Expedition 317 Drillsites, Canterbury Basin, New Zealand

BY

Faik Ozcan Polat, B.Sc.

Thesis

Presented to the Faculty of the Graduate School of

The University of Texas at Austin

in Partial Fulfillment

of the Requirements

for the Degree of

Master of Science in Geological Sciences

The University of Texas at Austin

December, 2012

DEDICATION

To my family and my fiancé, who have provided valuable support to enable me to accomplish my dream

ACKNOWLEDGEMENTS

I would like to start by thanking my supervisor Craig S. Fulthorpe for his valuable scientific insight and guidance. Not only his scientific support but also his inspiration and kindness encouraged me during my degree program. I am also indebted to my committee members, Professor William L. Fisher and Ronald J. Steel for their great support, valuable time, and suggestions. This thesis would never have been achievable without the financial support of Turkish Petroleum Corporation (TPAO). Lastly, my special thanks must go to Dallas Dunlap, Thomas Hess and Philip Guerrero for their invaluable technical support.

ABSTRACT

Core-Seismic Correlation and Sequence Stratigraphy at IODP Expedition 317 Drillsites, Canterbury Basin, New Zealand

Faik Ozcan Polat, MSGeoSci

The University of Texas at Austin, 2012

Supervisor: Craig S. Fulthorpe

High rates of Neogene sediment influx to the offshore Canterbury Basin resulted in preservation of a high-resolution record of seismically resolvable sequences (~0.1-0.54 my periods). Subsequent sequence development was strongly influenced by submarine currents. This study focuses on correlating seismically interpreted sequence boundaries and sediment drifts architectures beneath the modern shelf and slope with sediment facies observed in cores from shelf Site U1351 and slope Site U1352 drilled by Integrated Ocean Drilling Program (IODP) Expedition 317. A traveltime-depth conversion was created using sonic and density logs and is compared with two previous traveltime-depth conversions for the sites. Eleven large elongate drifts were interpreted prior to drilling. Two new small-scale plastered slope drifts in the vicinity of the IODP sites, together with sediment waves drilled at Site U1352, have been interpreted as part of this study. Lithologic discontinuity surfaces and transitions together with associated sediment packages form the basis of identifying sequences and sequence boundaries in the cores.

Contacts and facies were characterized using shipboard core descriptions, emphasizing grain-size contrasts and the natures of the lower and upper contacts of sediment packages. Lithologic surfaces in cores from sites U1351- (surfaces S1-S8) and U1352- (surfaces S1-S6) correlate with early Pleistocene to recent seismic sequence boundaries U12-U19 and U14-U19, respectively. The limited depths achieved by downhole logging, in particular sonic and density logs, together with poor recovery in the deeper section did not allow correlation of older lithologic surfaces. Slope Site U1352 experienced a complex interplay of along-strike and downslope depositional processes and cores provide information about the principal facies forming sediment waves. The general facies are fine-grained mud rich sediment interbedded decimeter-centimeter thick sand and sandy mud. Core evidence for current activity is reinforced at larger scale by seismic interpretations of sediment waves and drifts.

TABLE OF CONTENTS

LIST OF TABLES

LIST OF FIGURES

CHAPTER 1: INTRODUCTION

1.1 PREFACE

Integrated Ocean Drilling Program (IODP) Expedition 317 drilled in the offshore Canterbury Basin on the eastern margin of the South Island of New Zealand. The expedition recovered sediments with ages from Eocene to Recent. High rates of Neogene sediment supply produced a high-frequency (0.1-0.5 my) record of depositional cyclicity in the offshore basin (Lu & Fulthorpe, 2004). In addition, large sediment drifts occur within the Neogene section. These drifts were created by precursors of the modern Southland and Antarctic Circumpolar currents and significantly, modify sequence architecture. The drifts comprise large mounds (up to 1000 thick), oriented sub-parallel to the paleoshelf edge and present coastline, with channel-like moats at their landward edges (Fulthorpe & Carter, 1991; Lu et al., 2003). Expedition 317 therefore plays a crucial role in understanding sequence development on a continental margin which is strongly affected by along-strike currents (Fulthorpe et al., 2011).

The research described in this thesis involves 1) correlation of seismically interpreted sequence boundaries with sediment facies observed in cores and 2) a reevaluation of sediment drifts architectures using 2-D high resolution, multichannel seismic data.

This chapter outlines the study objectives, and summarizes previous work. Chapter 2 describes the geological background of region, including tectonic history, sedimentation and oceanographic settings. In chapter 3, I explain the role of along-strike sediment processes on this margin, and the distribution of sediment drifts, together with the methodology involved. Chapter 4, describes the lithologic discontinuity surfaces and transitions which, together with associated sediment packages, are the basis of identifying

sequences and sequence boundaries in the cores. I also describe the methodology for correlating these surfaces with seismic sequence boundaries. The final chapter contains discussion of results and conclusion.

1.2 STUDY AREA

The Canterbury Basin lies on the eastern side of South Island of New Zealand (Figure 1.1). The eastern part of the South Island is part of a continental fragment that includes the Campbell Plateau, Chatham Rise, and Bounty Trough. The Alpine Fault runs through the South Island and forms the boundary between the Pacific and Australasian plates (Figure 1.1). The Canterbury Basin extends from the Southern Alps eastward across the Canterbury Plains and covers a large area offshore. The total area of the basin is ~40,000 km^2 and it has been accumulating sediment since the Cretaceous when the margin rifted from Antarctica (~80 Ma; Molnar et al., 1975).

1.3 OBJECTIVE

This research focuses on the interplay of along-strike and downslope sediment transport and depositional processes on this current-swept margin. Firstly, this study focuses on constraining the role of currents in building the shelf/slope sediment prism and identifying the channel-like features and mounded geometries that are key components of drift architecture, as well as more subtle indicators of current activity, such as sediment waves using high resolution MCS profiles.

Second, this study correlates seismically interpreted sequence boundaries and sediment drifts with sedimentary surfaces observed in cores from Expedition 317 sites. Nineteen middle Miocene to Recent regional seismic sequence boundaries were interpreted using the EW00-01 data by Lu and Fulthorpe (2004) using standard seismic sequence stratigraphic techniques involving recognition of reflection terminations (e.g.,

onlap, truncation, downlap) and, in some parts of the section, shelf channel incisions. Lithologic discontinuity surfaces were identified in the cores during Expedition 317 and tentatively correlated with sequence boundaries by shipboard scientists (Fulthorpe et al., 2011). The method for identifying potential sequence boundaries in cores during Expedition 317 involved consideration of both individual surfaces and the overlying sedimentary package. Candidate lithologic surfaces were identified based on changes in lithologic composition across the contact, the presence of reworked sediments, and the nature of the contact (sharp versus gradational). A typical sediment package overlying such a lithologic contact involves fining-upward sediment above the contact followed by coarsening upward lithology (Fulthorpe et al., 2011). Correlations were tentative in part because basal contacts of some sediment packages were not recovered. In addition, there were more lithologic surfaces than seismic sequence boundaries; only surfaces close to the predicted depths of seismic sequence boundaries were examined. Finally, traveltime-depth conversion was uncertain during the cruise. Therefore, precise shipboard correlation of individual surfaces with seismic sequence boundaries was difficult.

These discontinuity surfaces and associated sedimentary packages have been reevaluated as part of this study using shipboard core descriptions, emphasizing grain-size contrasts (based on visual estimates) and the nature of the lower of sediment packages. This reevaluation supports the shipboard interpretations of some lithologic surfaces as sequence boundaries and changes the locations of other lithologic sequence boundaries. Reasons for changing lithologic sequence boundary locations are proximity to predicted seismic sequence boundary depth, based on the new traveltime depth conversions used for this study, and reinterpretation of some sediments above shipboard surfaces as cave-in.

Sites U1351, U1352 and U1353 are located continental shelf and Site U1352 is located on the upper slope. Correlation between seismic and core data requires time-depth conversion using downhole logging (e.g., sonic and density).

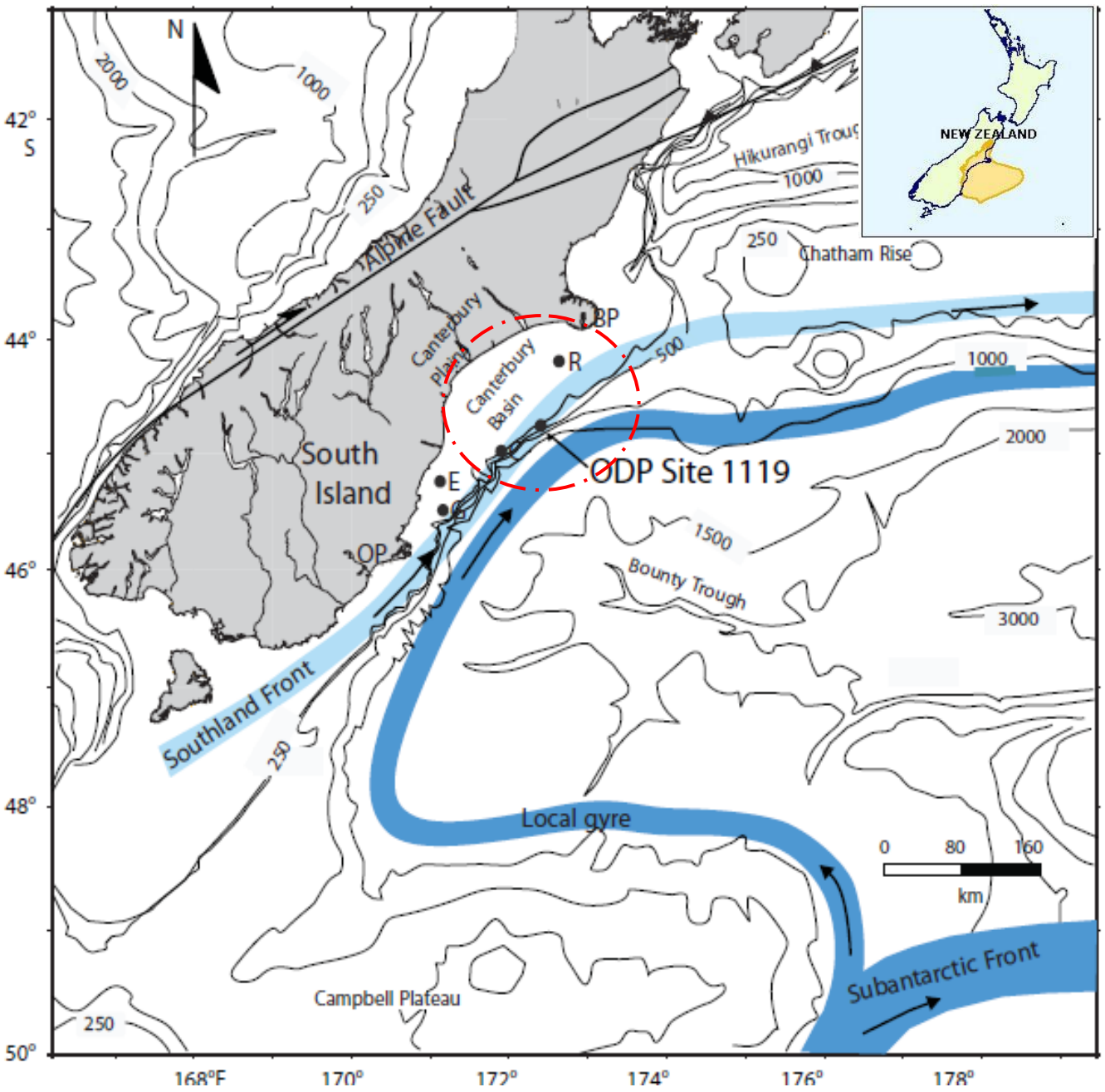

Figure 1.1: Location map showing Canterbury Basin (red circle) on the eastern margin of the South Island of New Zealand. The Alpine Fault is the boundary between Pacific and Australasian plates. E, Endeavour wells, C, Clipper, G, Galleon and R, Resolution together with ODP Site 1119 are shown on the offshore Canterbury Basin. Main oceanographic currents (Southland Front, Subantactic Front (SAF) and recirculated SAF as local gyre around the Bounty Trough) are also shown around New Zealand (Fulthorpe et al., 2011).

1.4 PREVIOUS WORK

Petroleum exploration in the Canterbury Basin was started with the Chertsey-1 well (Figure 1.2), drilled onshore to 660 m, between 1914 and 1921. Additional onshore wells J.D George-1 (1,650 m), Leeston-1 (2,714 m), and Kowai-1 (1,419 m) (Figure 1.2). However, beginning in the 1970s, the focus of hydrocarbon exploration in the Canterbury Basin shifted offshore. Four wells were drilled Enedeavour-1, Resolution-1, Clipper-1 and Galleon-1 but significant discoveries were made only in Galleon-1(3,086 m) and Clipper-1 (4,742 m) (Figure 1.2). A fifth well, Cutter, has been drilled more recently, but information about this well is not yet publically available.

During the last few decades, several commercial and academic seismic surveys have been collected both onshore and offshore reflecting increasing interest in the Canterbury Basin (Sutherland & Browne, 2003). Linking offshore observations to the onshore geology is essential to understanding of regional sedimentological evolution since the Cretaceous (Ballance, 1993). Academic research in the offshore basin has focused on the Neogene sedimentary response to sea level and ocean circulation and culminated in IODP Expedition 317 drilling (e.g., Fulthorpe & Carter, 1989; Fulthorpe & Carter, 1991; Fulthorpe et al., 1996; Fulthorpe et al., 2011; Lu & Fulthorpe, 2004; Lu et al., 2003). The work described in this thesis builds on the seismic interpretations of Lu et al. (2003) and Lu & Fulthorpe (2004), augmenting their interpretations of sediment drifts and correlating their sequence stratigraphic interpretations with the results of Expedition 317.

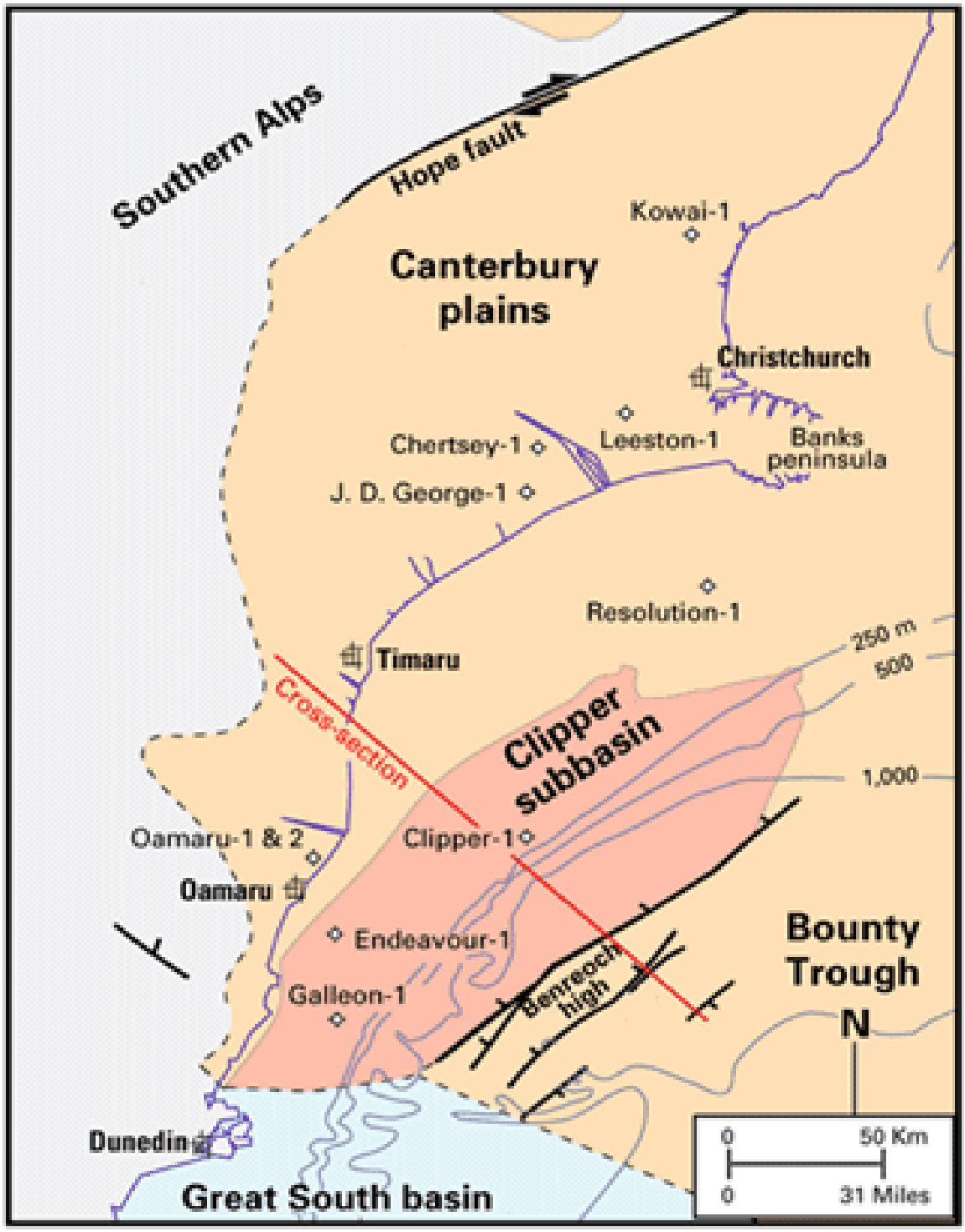

Figure 1.2: Onshore and offshore petroleum exploration wells in the Canterbury Basin (Sutherland & Browne 2003). The location of schematic cross section is shown in Figure 2.9.

CHAPTER 2: GEOLOGICAL BACKGROUND, DATA AND METHODOLOGY

2.1 TECTONIC HISTORY

The earliest tectonic history of the Canterbury Basin began with a Permian to Early Cretaceous convergent margin stage. However, in the mid-Cretaceous, New Zealand, Antarctica, and Australia began to separate in response to the break-up of Gondwana (Carter & Norris, 1976; Bradshaw, 1989; King, 2000; Wood & Stagpoole, 2007). From the Late Cretaceous to Oligocene, the Canterbury Basin was part of a passive margin (Sutherland & Browne, 2003; Fulthorpe et al., 2011). The Alpine Fault became active in the earliest Miocene (~23 Ma), adding tectonic complexity, and has since experienced > 450 km strike-slipe displacement (Kamp, 1986b; Wood & Stagpoole, 2007). Alpine Fault activity led to uplift and erosion of the Southern Alps, which accelerated at about 10 Ma and has led to the high rates of sediment supply to the offshore Canterbury Basin since late Miocene time (Sutherland & Browne, 2003).

2.1.1 Permian to Mid-Cretaceous

Most Permian to Early Cretaceous rocks were formed by convergent margin tectonics. The earliest basin architecture indicates an accretionary convergent margin setting (Figure 2.1), within which sediment was deposited and folded (Sutherland & Browne, 2003). The collision between the Pacific and Phoenix plates ended convergence in the Early Cretaceous (Bradshaw, 1989). This collision was followed by the initiation of separation of New Zealand from Antarctica and Australia in the mid-Cretaceous (Figure 2.2) (Molnar, 1975). Spreading along the Pacific-Phoenix ridge, the initial spreading center in the Tasman Sea and South of Australia, resulted in extensional tectonics in New Zealand. The Eastern Margin of the South Island of New Zealand rifted

from Marie Byrd Land in West Antarctica (~80 Ma; Molnar, 1975; Bradshaw, 1989) initiating the passive margin phase.

2.1.2 Late Cretaceous to Oligocene Passive Margin

During the passive margin phase, the New Zealand block experienced a period of relative tectonic stability with slow subsidence in the central part of the Canterbury Basin (Browne & Field, 1988). A widespread regional unconformity (~80 Ma), separates basal sediments from the overlying terrestrial and marine sediments (King, 2000; Bradshaw & Laird 2004). Post-rift transgression created a 1st order fining-upward sequence with terrestrial conglomerate, carbonaceous sandstone, siltstone and coal, overlain by marine sandstone and mudstone (King, 2000; Sutherland & Browne, 2003; Laird & Bradshaw, 2004). Continued subsidence and cessation of Tasman Sea spreading at about 52Ma (Figure 2.3) led to deposition of organic-rich black shales and carbonates during the Paleocene (King, 2000). The New Zealand sub-continent continued to drift away from Antarctica until the Middle Eocene (Kamp, 1986a; 1986b). The sub-continent was exposed to oblique separation and deformation during the late Eocene, but this deformation did not affect the Canterbury Basin (Molnar, 1975; Sutherland & Browne, 2003). Maximum transgression occurred during the Late Eocene and Early Oligocene (King, 2000; Sutherland & Browne, 2003).

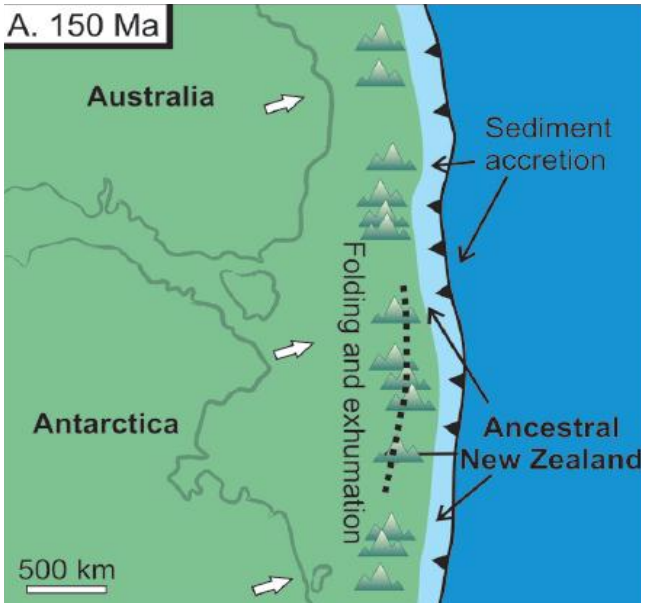

Figure 2.1: Reconstructed plate tectonic map of New Zealand at 150 Ma (Cox & Sutherland, 2007).

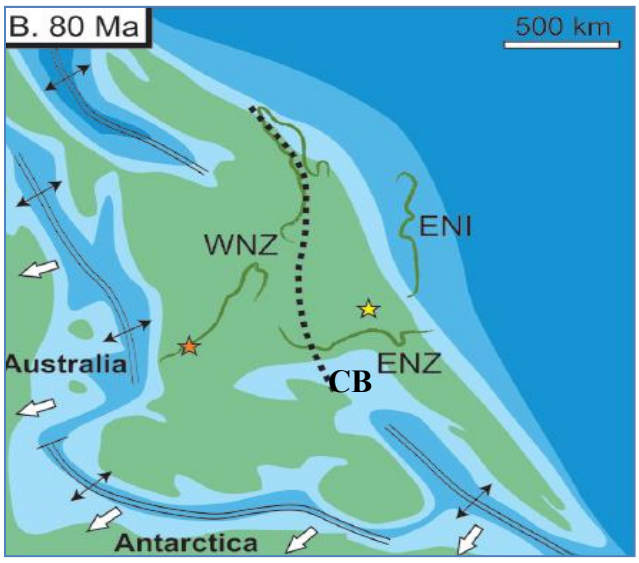

Figure 2.2: Reconstructed plate tectonic map of New Zealand at 80 Ma. Separation of the New Zealand from Antarctica and Australia plates began with Gondwana Break-up.WNZ=Western Province, ENZ=Eastern Province, ENI=Eastern North Island, CB=Canterbury Basin. The dashed line is the Junction Magnetic Anomaly, a prominent anomaly separating New Zealand terranes. (Cox & Sutherland, 2007).

2.1.3 Alpine Fault (Miocene to Recent)

The Canterbury Basin is located at the landward edge of the rifted continental fragment and underlines today's Canterbury Plains and offshore extensional continental shelf (Figure 2.6; King 2000; Lu et al., 2003). The predominantly strike slip (right lateral) Alpine Fault forms the boundary between the Australian and Pacific plates (Carter, 1976; Kamp, 1986b; King, 2000; Wood & Stagpoole, 2007). The west-oriented subduction along the North Island with oblique convergence and northwest-oriented oblique subduction of the South Island have resulted in transpressive movement on the Alpine Fault since the earliest Miocene (~23 Ma) (Figure 2.4; Norris et al., 2001; Wood & Stagpoole, 2007). Increasingly oblique convergence across the plate boundary resulted in deformation along the Alpine Fault and accompanying, uplift and erosion of the Southern Alps (Figure 2.5; Norris et al., 1990; Wood & Stagpoole, 2007). As a result, large volumes of clastic terrestrial sediment have been deposited in the offshore Canterbury Basin since the latest Miocene (Stagpoole, 2002; Sutherland & Browne, 2003).

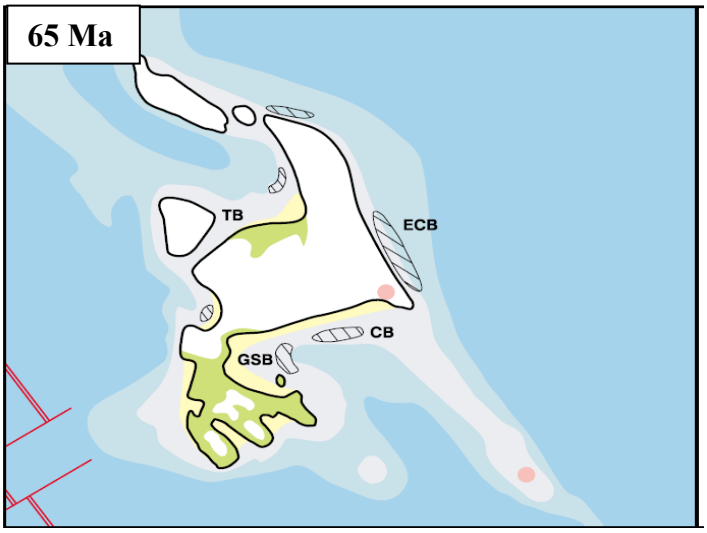

Figure 2.3: Reconstracted paleotectonic map of New Zealand at 65 Ma. Spreading in the Tasman Sea and South of Australia resulted in extensional tectonics in New Zealand. TB=Taranaki Basin, GSB=Great South Basin, ECB=East Coast Basin, CB=Canterbury Basin (King, 2000).

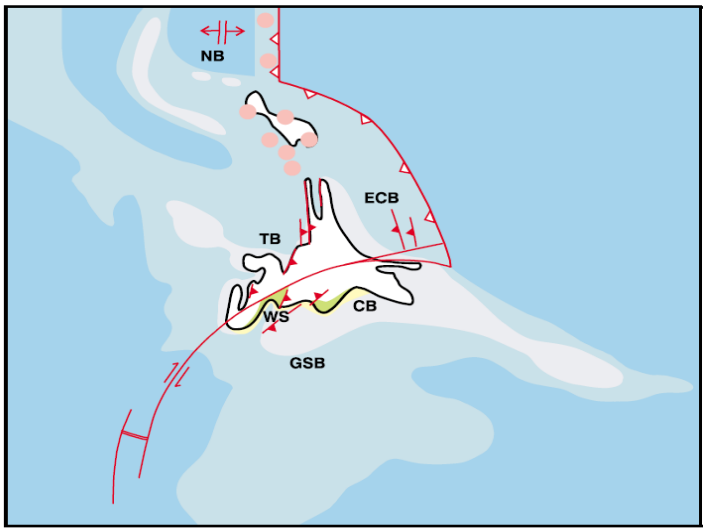

Figure 2.4: Reconstracted paleotectonic map of New Zealand at 20 Ma. Transpressive movement on the Alpine Fault and sea floor erosion began in the early Miocene. TB=Taranaki Basin, GSB=Great South Basin, ECB=East Coast Basin, CB=Canterbury Basin, PT=Puysegur Trench (King, 2000).

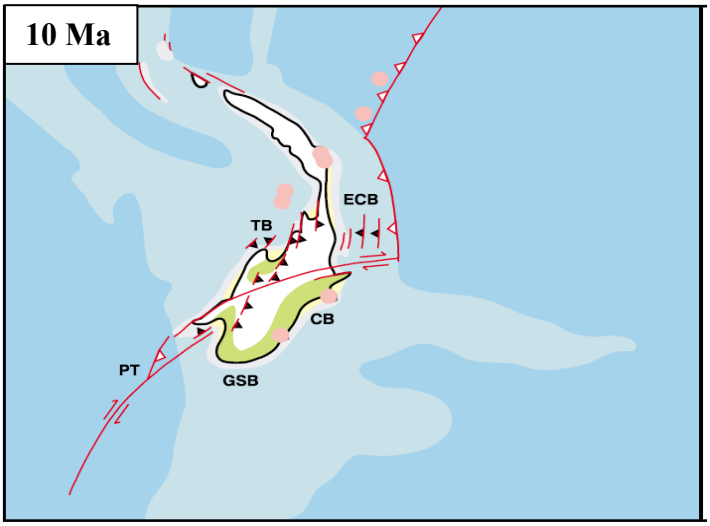

Figure 2.5: Reconstracted paleotectonic map of New Zealand at 10Ma. Increasingly oblique convergence across the plate boundary resulted in uplift and erosion in the Southern Alps. TB=Taranaki Basin, GSB=Great South Basin, ECB=East Coast Basin, CB=Canterbury Basin, PT=Puysegur Trench (King, 2000).

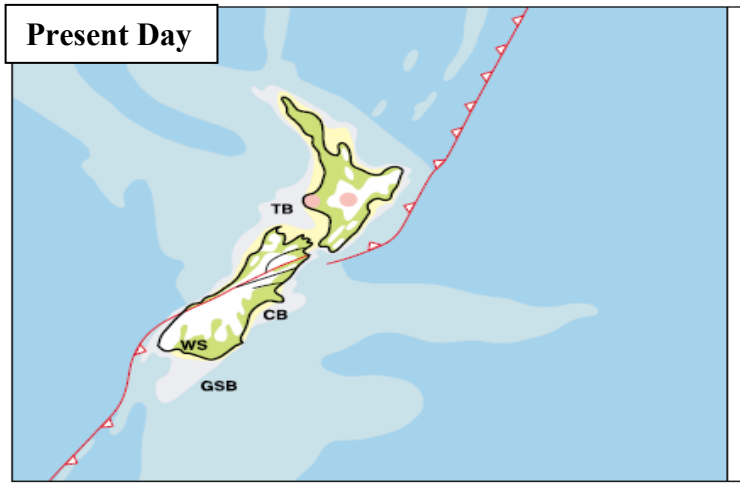

Figure 2.6: The present-day Canterbury Basin Transpression compression is ongoing in the South Island. TB=Taranaki Basin, GSB=Great South Basin, WS=Western Southland Basin, CB=Canterbury Basin (King, 2000).

2.2 SEDIMENTATION

The post-rift sedimentary history of the Canterbury Basin represents a first order, 80 my, transgressive-regressive cycle reflecting post-rift Cretaceous and Paleogene subsidence and flooding followed by siliciclastic progradation accompanying uplift and erosion along the developing Alpine Fault beginning in the Oligocene to early Miocene. The basin fill comprises the Onekakara, Kekenodon and Otakou groups (Figure 2.7; Lu et al., 2003).

Relative sea level rise during the Cretaceous-Oligocene marine transgression phase resulted in ramp-style, seaward dipping reflections (Figure 2.7; Fulthorpe et al., 1996). This fining-upward succession is composed of conglomerate, alluvial-fluvial sandstone, siltstone, and coal overlain by sandstone, siltstone and mudstone within the Onekakara Group (Sutherland & Browne, 2003). Marine transgression reached at a maximum during the Oligocene (Carter, 1988; Sutherland & Browne, 2003; Lu et al., 2003). The resulting restriction of siliciclastic input led to deposition of the late Eocene-early Oligocene (~30 Ma), pelagic to hemipelagic Amuri and Weka Pass limestones, and their equivalent formations, from wide-spread shallow marine platform to deep-water environments (Norris & Carter, 1976; Carter 1988; Fulthorpe et al., 1996; King, 2000; Sutherland & Browne, 2003; Fulthorpe et al., 2011). Deposition of carbonate-rich sediment occurred first in the northern part of the Canterbury Basin where the marine transgression began (King, 2000). The Marshall Paraconformity, hypothesized to result from enhanced thermohaline circulation associated with the initiation of the Antarctic Circumpolar Current (ACC) between Antarctica and Australia, occurs at the top of the Amuri Limestone and is overlain by the thin authigenic Concord Formation and the Weka Pass Limestone, collectively comprising the condensed Kekenodon Group (Fulthorpe et al., 1996; Carter et al., 2004) (Figure 2.7).

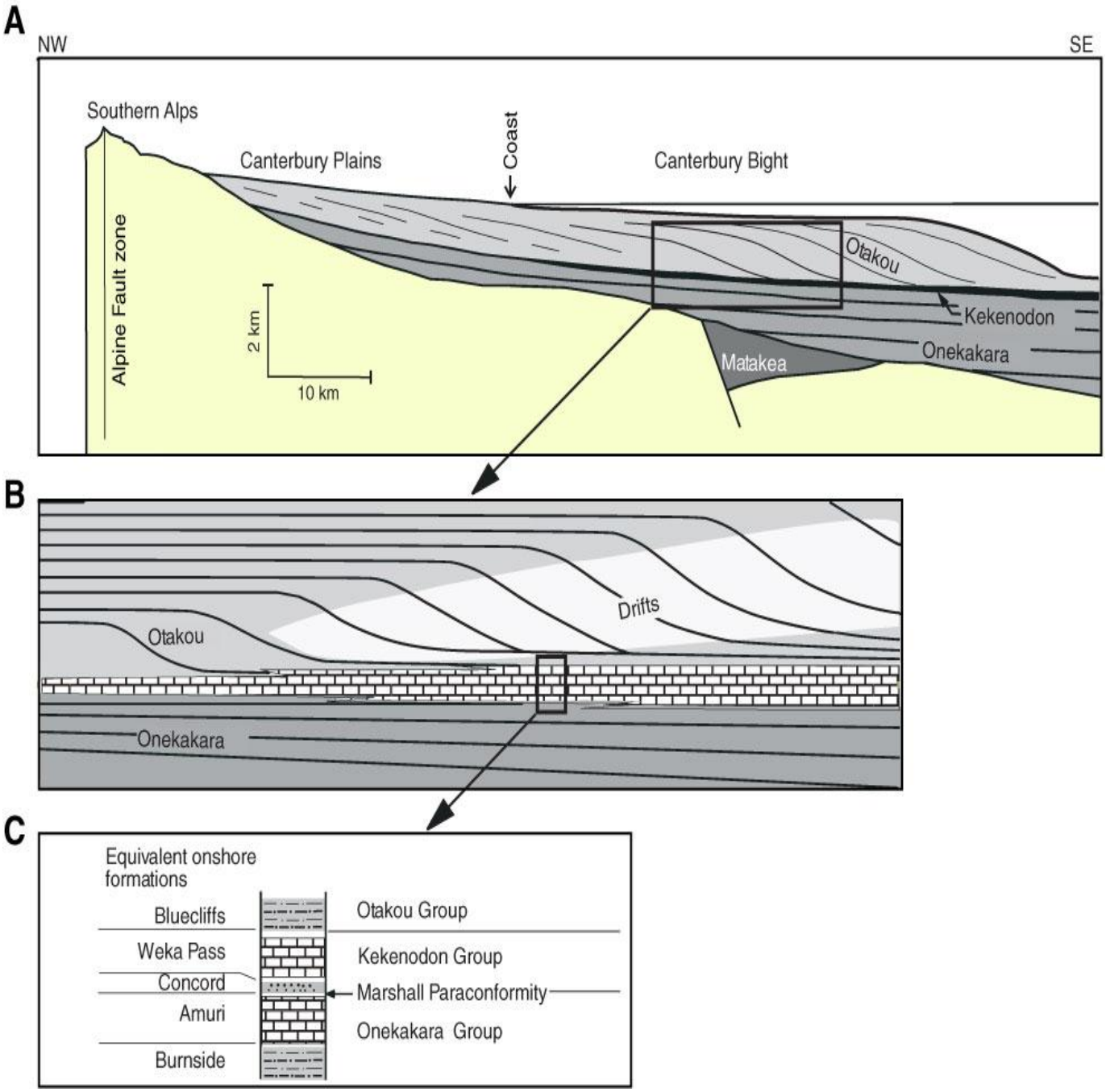

Figure 2.7: Stratigraphic diagrams of the Canterbury Basin are shown with three different displays. (A) Large-scale, deposition of the Onekakara, Kekenodon, Otakou groups are shown as a post-rift phase. (B) Seismic-scale stratigraphy. The transgressive Onekakara group underlies the pelagic to hemipelagic limestone unit and the regressive Otakou group in which sediment drift develops. (C) Outcrop-scale, cross-section stratigraphy of the Canterbury Basin (after Fulthorpe et al., 1996).

Development of the modern plate boundary and transpressive motion at the Alpine Fault caused uplift and erosion on the South Island. The resulting influx of siliciclastic sediments initiated the regressive phase of deposition. The Neogene sediment influx accumulated as the progradational Otakou Group (Figure 2.7) in the offshore Canterbury Basin (Carter, 1998; Lu et al., 2003). Eastward progradation occurred at rates between 1.5 and 4.9 km/my (Carter, 1988). The Otakou Group is composed predominantly of terrigenous siltstone with intermittent fine to very fine sand and mud at offshore exploration wells Clipper (Hawkes and Mound, 1985), Galleon (Wilson, 1985) and Endeavour (Wilding and Sweetman, 1971) (Figure 1.2). In addition, recent offshore coring by Expedition 317 (Figure 3.1) at Sites U1351, U1352, U1353 and U1352 showed that the Otakou Group also contains marly calcareous beds (Fulthorpe et al., 2011). Fulthorpe and Carter (1989) published the first sequence stratigraphic interpretation of the Neogene section using low-resolution oil-industry seismic data. Collection of high-resolution multichannel seismic data in January 200 (cruise EW00-01) led to a revised sequence stratigraphy. Lu and Fulthorpe (2004), identified nineteen Miocene to Recent regional sequence boundaries and 14 local unconformities. In addition, large sediment drifts have developed within the Otakou Group since the early Miocene reflecting the continued importance of currents to sediment transport and deposition (Fulthorpe & Carter, 1991; Fulthorpe et al., 1996).

2.3 OCEANOGRAPHIC SETTING

The Southland Current flows northeastward along the modern margin (Figures 1.1 and 2.8). The current is a branch of the Subtropical Front, which flows around the southern end of the South Island and up the east coast (Figure 2.8; Heat, 1972; Heat 1981; Morris, 2001). The warm and saline Southland current, is constrained by the shallow bathymetry of the eastern South Island coastline (maximum depth of 580 m) and

the Chatham Rise (at 1000 m depth) and flows northwestward through the Mernoo Gap (Figures 1.1 and 2.8; Heat, 1972). The colder and fresher Subantarctic Front (SAF) forms the eastward boundary of Southland Current (Figure 1.1; Morris, 2001). The SAF is the northern boundary of the Antarctic Circumpolar Current (Figure 1.1; Heat, 1981; Morris et al., 2001). However, the SAF is deflected westward on the northern side of the Campbell Plateau and recirculated as a local gyre around the head of Bounty Trough (Figure 1.1; Morris et al., 2001). The Canterbury Basin Neogene sedimentary system, building both large and small scale sediment drifts within the Otakou Group since the late Miocene, shows that the basin has long been influenced by precursors of the SAF and Southland Current systems (Figure 2.7; Fulthorpe and Carter, 1991; Fulthorpe et al., 1996; Morris, 2001; Lu et al., 2003). At least eleven large elongate drifts formed within the Otakou Group near the slope toe and aggraded to upper-slope water depths (Lu et al., 2003). The Neogene shelf sediment prism within the Otakou Group prograded in part by accretion of successive sediment drifts (Fulthorpe and Carter, 2001; Lu et al., 2003).

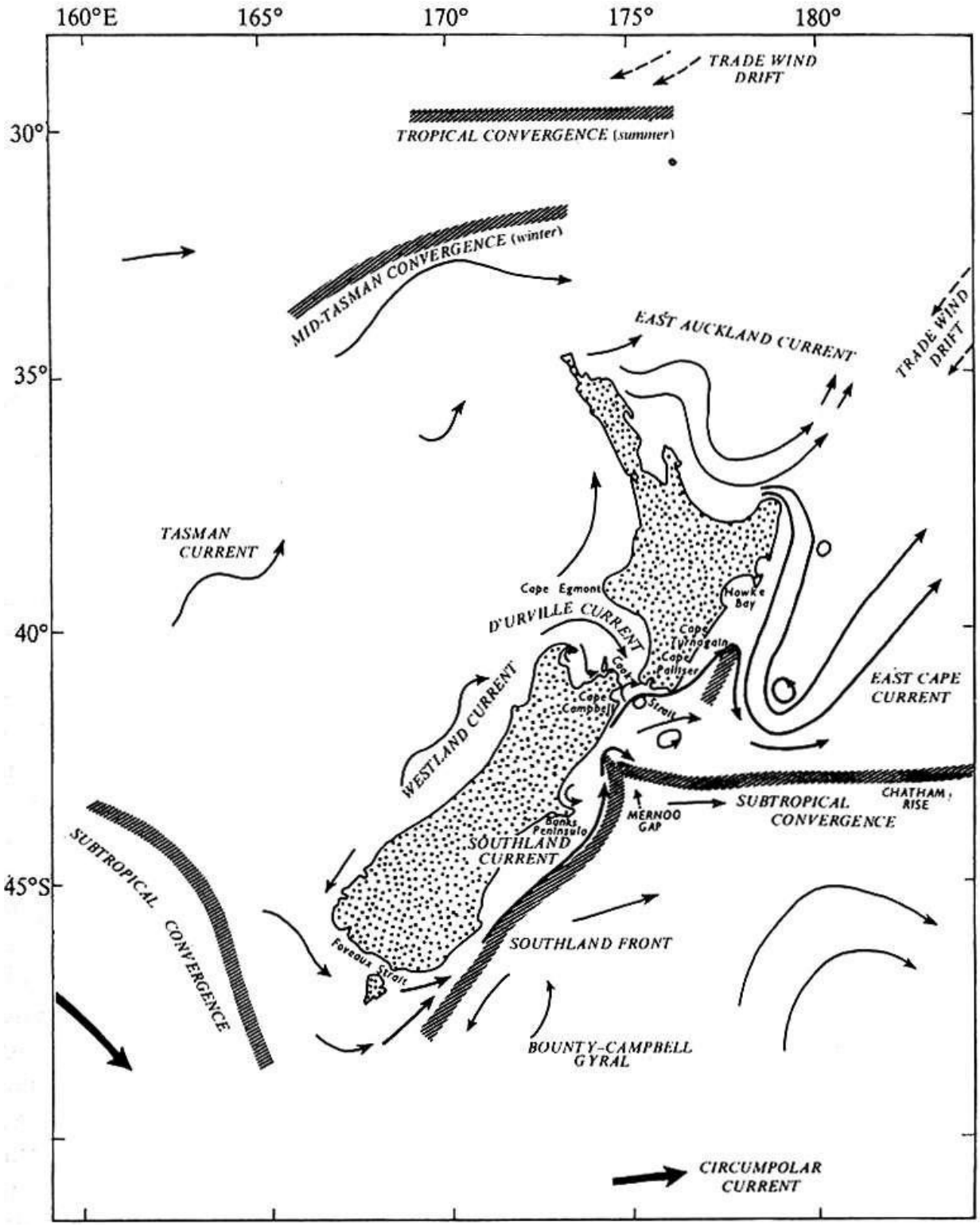

Figure 2.8: Main oceanographic currents are shown around New Zealand (Heat, 1972).

2.4 DATA

2.4.1 Multichannel High Resolution 2-D Seismic Data

Two-dimensional high resolution MCS seismic data acquisition was carried by R/V *Maurice Ewing* (cruise EW00-01) in January 2000. The survey area lies between the Banks and Otago Peninsulas on the middle to outer shelf and slope (Figure 2.9). The seismic source comprised two GI air guns (45/45 in^3) and the streamer was configured in 96 and 120 channel receiver groups with a 12.5 m group interval. The survey collected 57 profiles covering an area of 4840 km^2 (Figure 2.9). Line spacing varies from 0.7 km to >3 km in the dip direction and 2 km to >5.5 km in the strike direction. The GI guns provided a high-frequency source with frequencies of 100-500 Hz. This yielded vertical resolution of ~5 m in the upper second of two-way travel times. The record length was 3 seconds and the data were sampled at 1 ms to avoid aliasing. Resolution in the upper 1.7- 2.0 s below sea floor was sufficient to interpret geological features (e.g., sequence boundaries and sediment drifts) within the Oligocene to Recent section. The data were processed post-cruise using Focus software (processing parameters are shown in Table 2.1). For this project, the MCS data were interpreted in using Landmark seismic interpretation software version 50000.1.2.

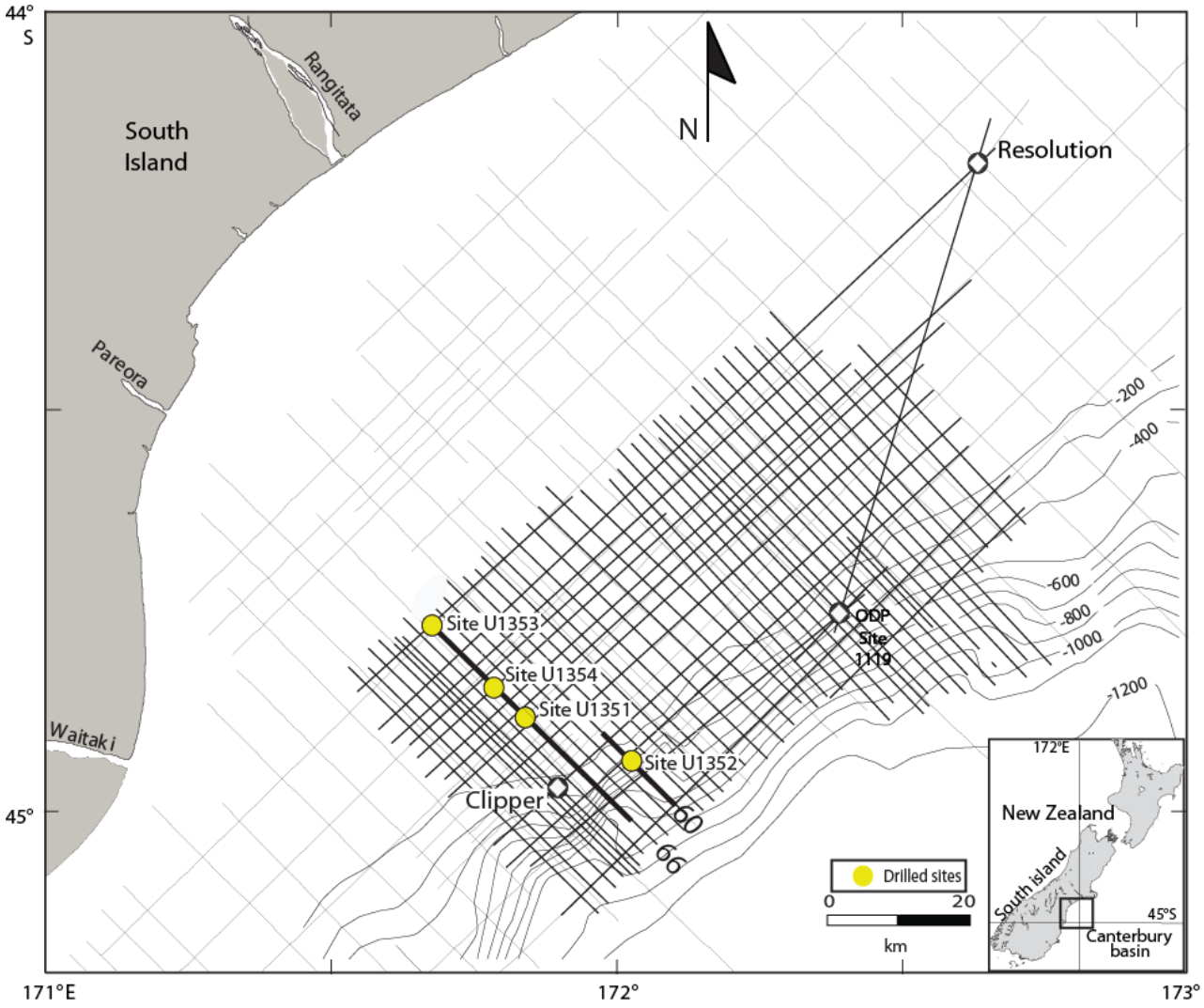

Figure 2.9: EW00-01 seismic grid IODP Expedition 317 drilled Sites U1351, U1352, U1353, and U1354 are shown (yellow dots), as are preexisting exploration wells Clipper, Resolution and ODP Site 1119.

Table 2.1: Data processing steps for the EW00-01 seismic data with Focus processing software functions.

Data processing	Focus Function
Read and reformat field data from tape	[GIN, IN,DSKRD]
Recover amplitude loss due to geometric spreading and frequency attenuation	t^2
Remove frequency-differentiable noise	[FILTER] 5-10-200-230
Remove bad traces	[EDIT] delete channel 19
Geometry	[PROFILE]
CDP gather sorting	[SORT]
Deconvolution	[DECONV] [FKFILTER]
Normal moveout	[NMO]
Remove post-critical and stretched or distorted energy	[MUTE]
Lateral amplitude balance	[BALANCE]
CDP stack	[STACK]
F/K migration	[F/KMIG]
Save result	[DSKWRT]
Improve display	[FILTER,AGC]
Plot	[DECPLOT]

2.4.2 Borehole Data

IODP Expedition 317 drilled Middle Miocene to Recent sequences at four sites: Sites U1351, U1352 and U1353 are located on the continental shelf and Site U1352 is located on the upper slope (Figure 2.10 A and B). Site U1351 is situated on the outer shelf in a water depth of 122 m and is located on dip seismic profile EW00-01-66 (Figure 2.10 A). Three holes were drilled at this site (Holes U1351A, U1351B, and U1351C). Maximum penetration was 1030.6 m at Hole U1351B. The advanced piston corers (APC), extended core barrel (XCB) and rotary core barrel (RCB) were deployed in an effort to maximize recovery. Much of the section was poorly lithified and IODP has historically found such sediments difficult to recover. Therefore, total recovery varies with holes condition; 27.3 m and 304.5 m were recovered from the 28 m and 1030.6 m penetrated in Holes U1351A and U1351B, respectively. Hole U1351C was drilled as a logging hole and was not cored (Table 2.2). Site U1352 lies on the upper slope (344 m water depth) on dip profile EW00-01-60 (Figure 2.10 B). Four holes were drilled at this site. Maximum penetration was 1927.5 m at Hole U1352C**.** Recovery was 43.9 m at U1351A (42.2 m penetration), 613.9 m at U1352B (830.9 m penetration), 655 m at U1352C (1927.5 m penetration) and, 130.8 m at U1352D (127 m penetration) (Table 2.2). Site U1353 is located on the middle shelf on dip Profile EW00-01-66 (Figure 2.10 A). This was the shallowest water site drilled during Expedition 317 with a water depth of only 85 m. Lastly, Site U1354 was also drilled on the middle shelf in a water depth of 113 m. Site U1354 is located on at the intersection of strike profile EW00-01-01 with dip profile EW00-01-66 (Figure 2.10 A). Detailed information on site locations, penetrations and recovery are given in Table 2.2. This project focuses on Sites U1351 and U1352 because of the availability of sonic logs for time/depth conversion to facilitate core/seismic correlation. Data from Sites U1353 and U1354 were not used for

core/seismic correlation because poor holes condition limited the effectiveness of the logging programs at those sites.

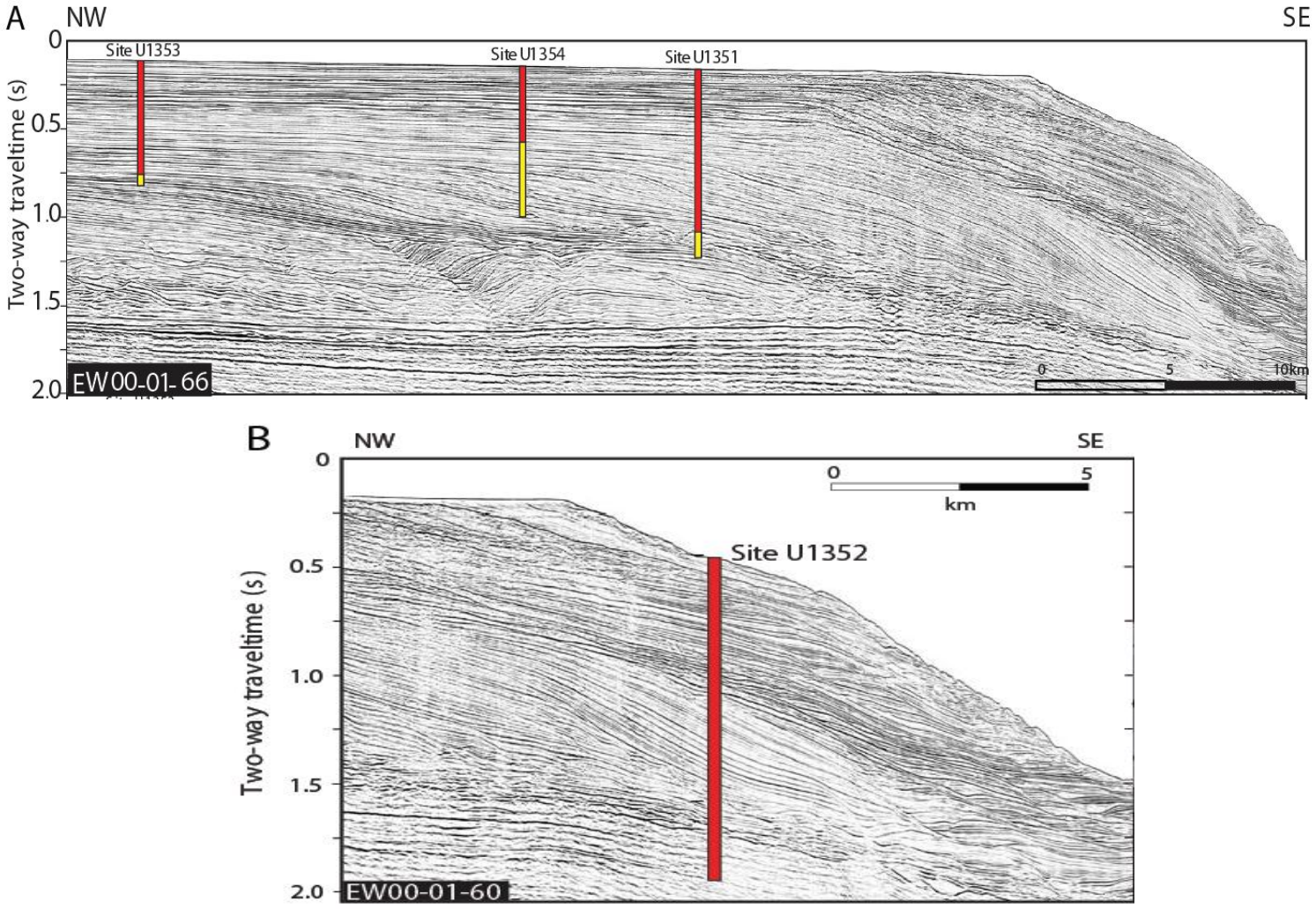

Figure 2.10: (A) Uninterpreted MCS profile EW00-01-66 showing Sites U1351, U1353 and U1354 overlain the seismic profile and current and anticipated penetrations with red and yellow bar. (B) MCS profile EW00-01-60 showing also Sites U1352 overlain the seismic profile and current penetrations with red bar.

Table 2.2: Summary of the drilling sites, Expedition 317.

Sites	Hole	Position	Water depth (m)	Total penetration (m)	Total core recovered (m)	Core recovery (%)	Total number of cores
Site U1351	U1351A	44°53.0307'S 171°50.4037'E	122.3	28	27.3	98	6
	U1351B	44°53.0422'S 171°50.4065'E	121.7	1030.6	304.5	30	116
	U1351C	44°53.0472'S 171°50.4057'E	121.7	967.3	0	0	0
Site U1352	U1352A	44°56.2440'S 172°1.3615'E	343.8	42.2	43.9	104	5
	U1352B	44°56.2558'S 172°1.3630'E	343.6	830.9	613.9	74	94
	U1352C	44°56.2662'S 172°1.3630'E	343.5	1927.5	655	51	148
	U1352D	44°56.2326'S 172°1.3611'E	344.2	127	130.8	103	14
Site U1353	U1353A	44°46.1079'S 171°40.4368'E	84.2	56	56.4	101	8
	U1353B	44°46.1203'S 171°40.4407'E	84.7	614.3	211.5	34	98
	U1353C	44°46.0982'S 171°40.4380'E	84.7	529	0	0	0
Site U1354	U1354A	44°50.8281'S 171°47.2096'E	109.8	85.4	84.4	101	19
	U1354B	44°50.8367'S 171°47.2069'E	113.4	77.2	77.5	100	15
	U1354C	44°50.8487'S 171°47.2080'E	113.4	384.2	133.4	42	36

2.5 METHODOLOGY

2.5.1 Seismic Interpretation of Drift Architecture

This first goal of this study focuses on constraining the role of currents in building the sediment prism that lies beneath the modern shelf and slope. The high resolution MCS profiles play as crucial role in identifying the channel-like features and mounded geometries that are key components of drift architecture, as well as more subtle indicators of current activity, such as sediment waves. Reflection amplitudes also vary within drifts from low amplitude at drift bases to medium amplitude at crests and discontinuities identified by reflection truncation are common features of internal drift geometries. Seismic interpretation has allowed the identification and mapping of two small-scale elongate and complex drifts that have not previously been recognized. These new drifts are in addition to the eleven elongate drifts originally identified by Lu et al. (2003) and Lu & Fulthorpe (2004).

2.5.2 Identification of Lithologic Surfaces in Cores Based on Predicted Sequence Boundary Depths

A second goal is to correlate seismically interpreted sequence boundaries and sediment drifts with sedimentary surfaces and lithologies identified in cores from Expedition 317. Nineteen middle Miocene to Recent regional seismic sequence boundaries were interpreted using the EW00-01 data by Lu and Fulthorpe, 2004. Lithologic discontinuity surfaces and their associated sediment facies were identified in the cores during Expedition 317 and tentatively correlated with sequence boundaries by shipboard scientists (Fulthorpe et al., 2011). These discontinuity surfaces and associated sedimentary packages have been verified as part of this study using shipboard core descriptions, emphasizing grain-size contrasts (based on visual estimates) and the nature of the lower and upper contacts of sediment packages.

2.5.3 Core-Seismic Correlation

Correlation between core and seismic data requires conversion between seismic two-way traveltime and depth below sea-floor. Therefore, in order to assure a more precise match between seismic and core data travel-time depth conversions were created for holes U1351B and U1352B from sonic and density logs collected during Expedition 317 using the Landmark suite's Syntool. These traveltime-depth conversions were then compared with two previous conversions created by Lu & Fulthorpe (2004) and Brusova (2010) (Figures 2.12 and 2.13).

Sonic and density logs are collected as functions of depth in borehole. The density log uses a gamma-ray source and formation density is derived from the amount of back-scattered radiation. Sonic velocity within the borehole walls is determined by measuring the time taken for sound to travel between a downhole source and receiver.

Both the sonic and density logs are employed to calculate acoustic impedance for each subsurface layer. The acoustic impedance, *I*, is given by the following equation:

$$I = V(velocity) \times \rho(density) \tag{3.1}$$

The reflection coefficient, *R*, is then calculated for the nth interface, assuming P-wave reflection at zero offset and is defined by the equation:

$$R_n = \frac{I_1 - I_0}{I_1 + I_0}, \tag{3.2}$$

where I_1 and I_0 are the impedances above and below the interface, respectively.

Finally, the reflection coefficient curve obtained from equation (3.2) is convolved with a representative wavelet to generate a synthetic seismogram using Syntool. This convolution can be represented as:

$$S(t) = R(t) * w(t) \tag{3.3}$$

Where w(t) represents the seismic wavelet. And, S(t) represents the synthetic seismogram.

Based on the explanation above, in creating synthetic seismograms I used either the sonic and density logs alone or both together. Both the amplitude and phase spectrum of the source wavelet for the synthetic seismogram can be predicted from the seismic data. The calibration of sonic log and density logs for U1351B and U1352B were made relative to the sea floor taking into account that zero time reflection is the sea level and that the Kelly bushing elevation is 11 m above sea level. In this section, I explain the time-depth conversion for U1351B in this chapter as a representative example. The same procedure was used for Hole 1352B. At shelf Hole U1351B, a sonic log was obtained to 488 m and a density log to ~1030 m below sea floor. In contrast, at slope Hole U1352B, logging depths were 442 m for sonic and 497 m for density. I created a time-depth conversion synthetic seismogram covering the full penetration of Hole U1351B (1030 m). For the interval below the maximum depth of the sonic log (490 m), the synthetic seismogram was estimated using inverse Gardner relationship because this relationship predicted sonic log from density log for the interval below maximum depth of the sonic. I created synthetic seismogram using both a zero-phase wavelet (Figure 2.10 panel 7) in the frequency range 30-80 Hz with 10 sec length of sweep and mix-phase wavelet (Figure 2.11 panel 9). The choice of wavelet changes the appearance of the synthetic seismogram (Bacon et al., 2003). For this reason, I used both zero-phase and mix-phase wavelets to

evaluate the differences between them and obtain the best fit with seismic profile EW0001-66. Although the mix-phase wavelet enhances the visual match, it also matched the noise in seismic. Therefore, the zero-phase wavelet was determined as the best match wavelet when overlain on traces 4305-4315 from profile EW00-01-66 (Figure 2.14).

Figure 2.11 shows an example Syntool display to create synthetic seismogram using sonic and density logs derived from Hole U1351B. The scale on the left-hand side includes both depth in meters and two-way travel-time in milliseconds. The next five tracks display sonic, density, seismic impedance, reflection coefficient, and synthetic seismogram logs, respectively. The time-depth conversions derived from synthetic seismograms for U1351B and U1352B are shown by the green curves in Figures 2.12 and 2.13 and were used to estimate sequence boundary depths.

An alternative time–depth conversion was derived prior to Expedition 317 by Lu (2004) and used to predict depths to sequence boundaries in advance of drilling. This time-depth relation was derived from check-shot and sonic log data from the Clipper exploration well and ODP Site 1119 (Figure 2.9) and resulted in the following equation:

$$Y = 316.99X^2 + 758.34X \qquad (3.4)$$

where Y is depth in meters below sea floor and X is two-way travel-time in seconds. This precruise function is plotted on Figures 2.12 and 2.13 (blue curves) for Sites U1351B and U1352B.

Time-depth conversions for U1351B and U1352B were also created independently by Brusova (2010) based on compaction characteristics and porosity trends together with lithologic information for sand, silt and clay. Using these properties,

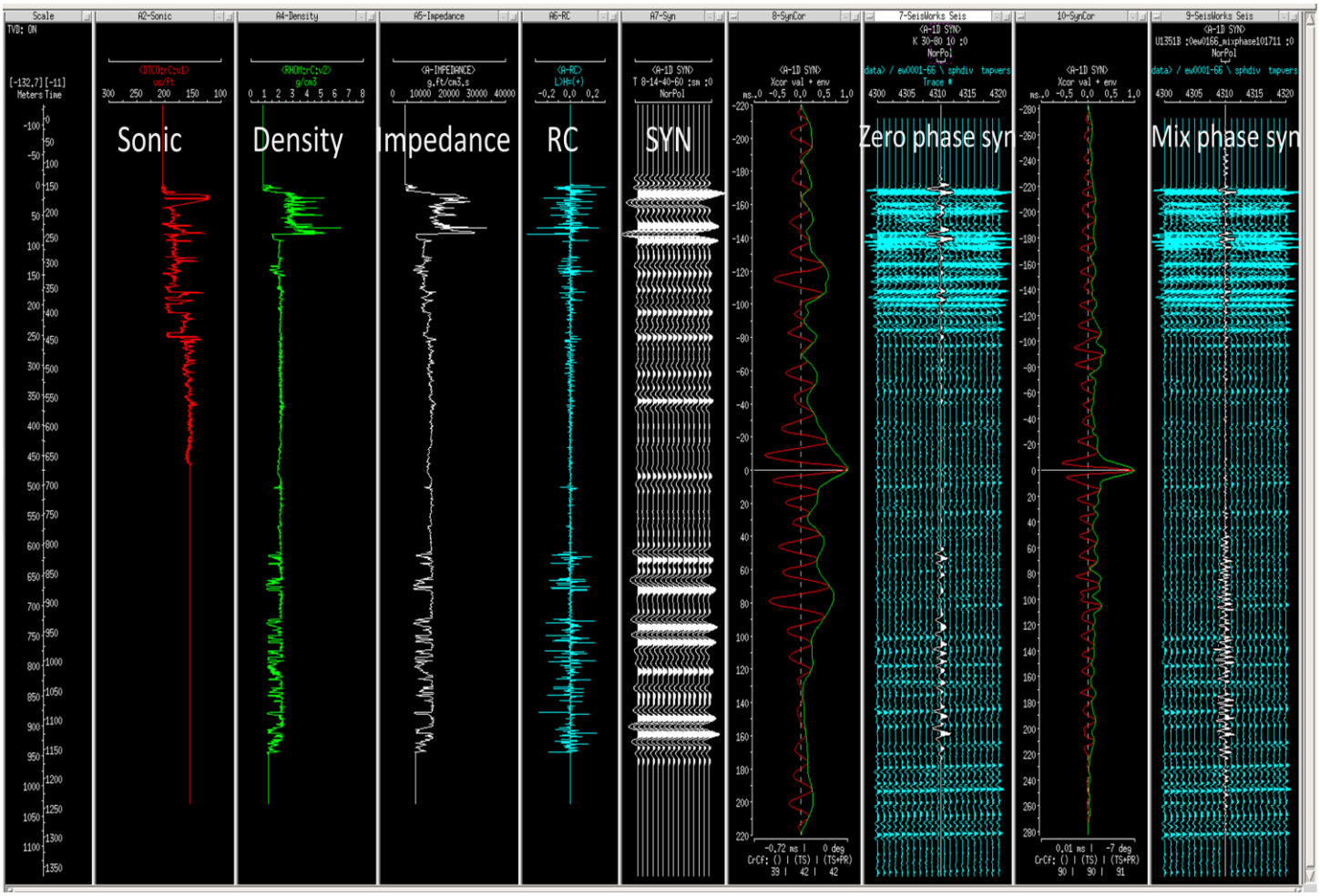

Figure 2.11: The generation of a synthetic seismogram using sonic and density logs derived from U1351B. From left to right, successive tracks represent: time/depth scale, sonic log, density log, calculated impedance log, calculated reflection coefficient log, synthetic overlain on traces 4305-4315 from profile EW00-01-66 for zero-phase wavelet with its envelope, and mix-phase wavelet with its envelope, respectively.

Brusova, (2010) determined velocity models for the U1351B and U1352B, and, the results were represented as 3rd order polynomial functions for U1351B and U1352B. These are shown in Figure 2.12 and 2.13 (red curve) and given by the following equation:

$$Y = 1.28X + (-4.22E^{-4})X^2 + 1.32E^{-7}X^3 (U1351B) \quad (3.5)$$

$$Y = 1.30X + (-4.52E^{-4})X^2 + 0.77E^{-7}X^3 (U1352B) \quad (3.6)$$

where Y is two-way travel-time in seconds and X is depth in meters below sea floor.

Figures 2.12 and 2.13 compare the synthetic-derived traveltime-depth curve (green), the precruise function (blue) and Brusova (2010) curves (red). The location of sequence boundaries for each curve are also shown in Figures 2.12 and 2.13 The curve derived from the synthetic yields lower depths than the other over most depth ranges. The fact that the Brusova and precruise function seem to flip between U1351 and U1352 is interesting, but this is seen only in the deepest part of the section: the curves in the upper 1000m of U1352 are consistent with U1351. The precruise function was designed to overestimate depths to provide conservative drilling time estimates. However, it apparently fails at depth in U1352, where it not "fast enough" and underestimates depths relative to Brusova (2010) and indeed relative to the stratigraphy: the MP was deeper than expected. Brusova, (2010) referred that the MP was located at 1380 msec in TWT seismic and at 1853 m below sea-floor corresponds to actual drilling result of U1352. Unfortunately, poor hole condition at Site U1352 prevented logging beyond a depth of 442 m so that no synthetic-derived traveltime-depth conversion was possible for the deeper section, including the MP.

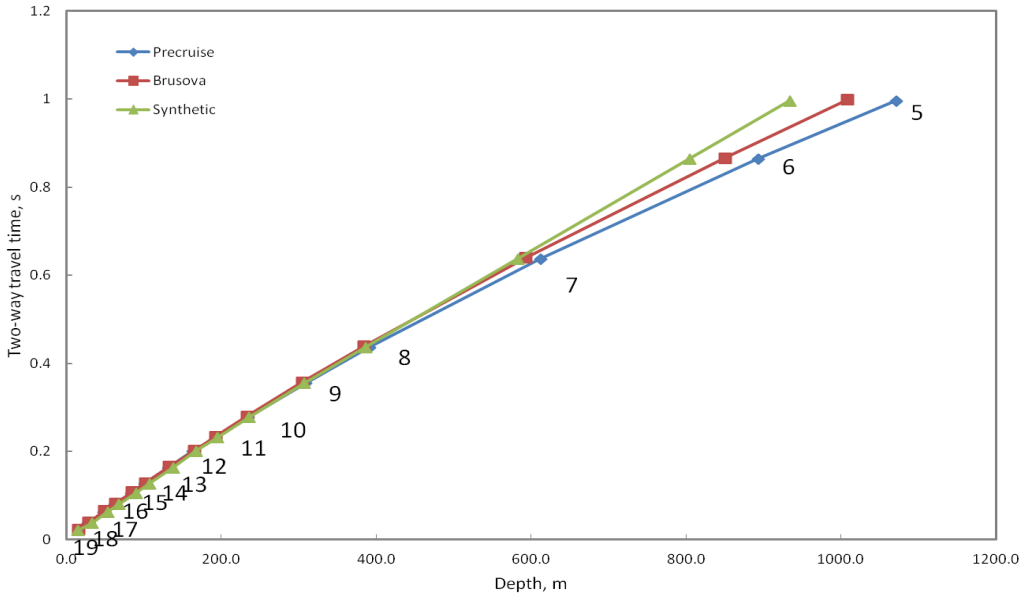

Figure 2.12: Comparison of the three different time-depth conversions for Hole U1351B. Sequence boundaries are marked and labeled: Precruise (blue diamond), Brusova (red square), and Synthetic (green triangles).

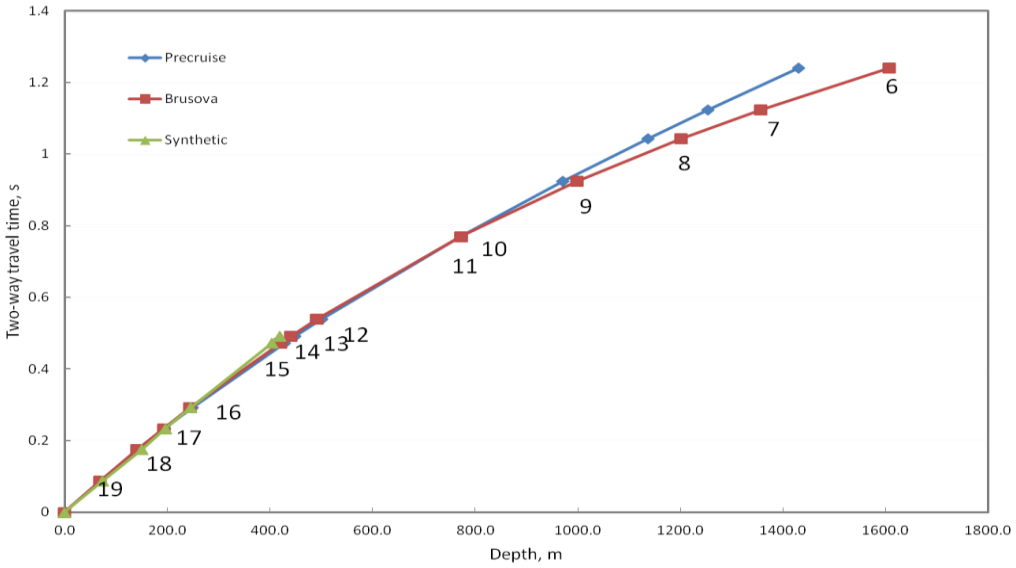

Figure 2.13: Comparison of the three different time-depth conversions for Hole U1352B. Each sequence boundaries are marked and labeled: Precruise (blue diamond), Brusova (red square), and Synthetic (green triangle).

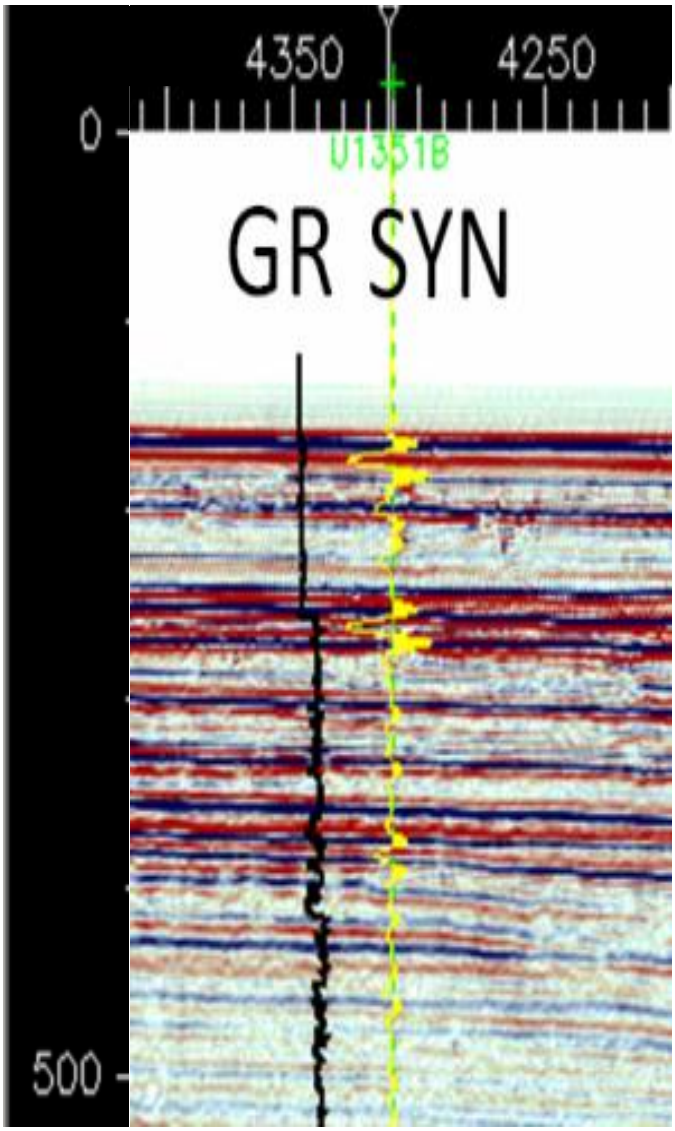

Figure 2.14: Synthetic seismogram for Hole U1351B overlain on seismic profile EW01-00-66 at trace 4310. The gamma-ray log is also shown at the location of U1351B.

CHAPTER 3: SUCCESSION OF SEDIMENT DRIFTS AND WAVES AND LOCAL CONTROLS ON SEQUENCE FORMATION IN THE CANTERBURY BASIN (EW00-01 STUDY AREA)

3.1 DRIFT DEPOSITS IN THE STUDY AREA

Lu et al. (2003) interpreted 11 large-scale sediment drifts within the early Miocene to recent section in the offshore Canterbury Basin (Figure 3.1). They identified the drifts as elongate drifts based on the classification developed for late Eocene/Oligocene drifts in northwestern Britain by Stoker et al (1998). A schematic illustration of elongate drift seismic characteristics is shown in Figure 3.2. The Canterbury drifts were initiated at paleoslope toes, in 300-750 m water depth and formed in response to a current flowing northeastward along the margin. The drifts feature mounded morphologies with moats along their landward flanks. Lu et al. (2003) also subdivided the drifts based on their internal architectures, into two groups: simple and complex. The oldest drifts are small simple drifts (D1-D6) and occur in the southern part of survey area (Figure 3.1). The locus of drift deposition migrates northeastward through time so that the youngest drifts D10 and D11 occur in the northeastern part of the survey area (figure 3.1). These youngest drifts are also simple and are the largest drifts in the basin: increase in size through time in response to increasing accommodation space basinward of the paleoslope in response to the aggradation of the shelf/slope sediment prism. D7- D9 are complex drifts of intermediate size (Figure 3.1). Complex drifts can be further subdivided into multi-crested and multistage drifts: multi-crested drifts display lateral shifting of the moat, possibly in response to sea-level fluctuations, whereas multi stage drifts may represent fluctuations in the rate of sediment supply (Lu et al., 2003).

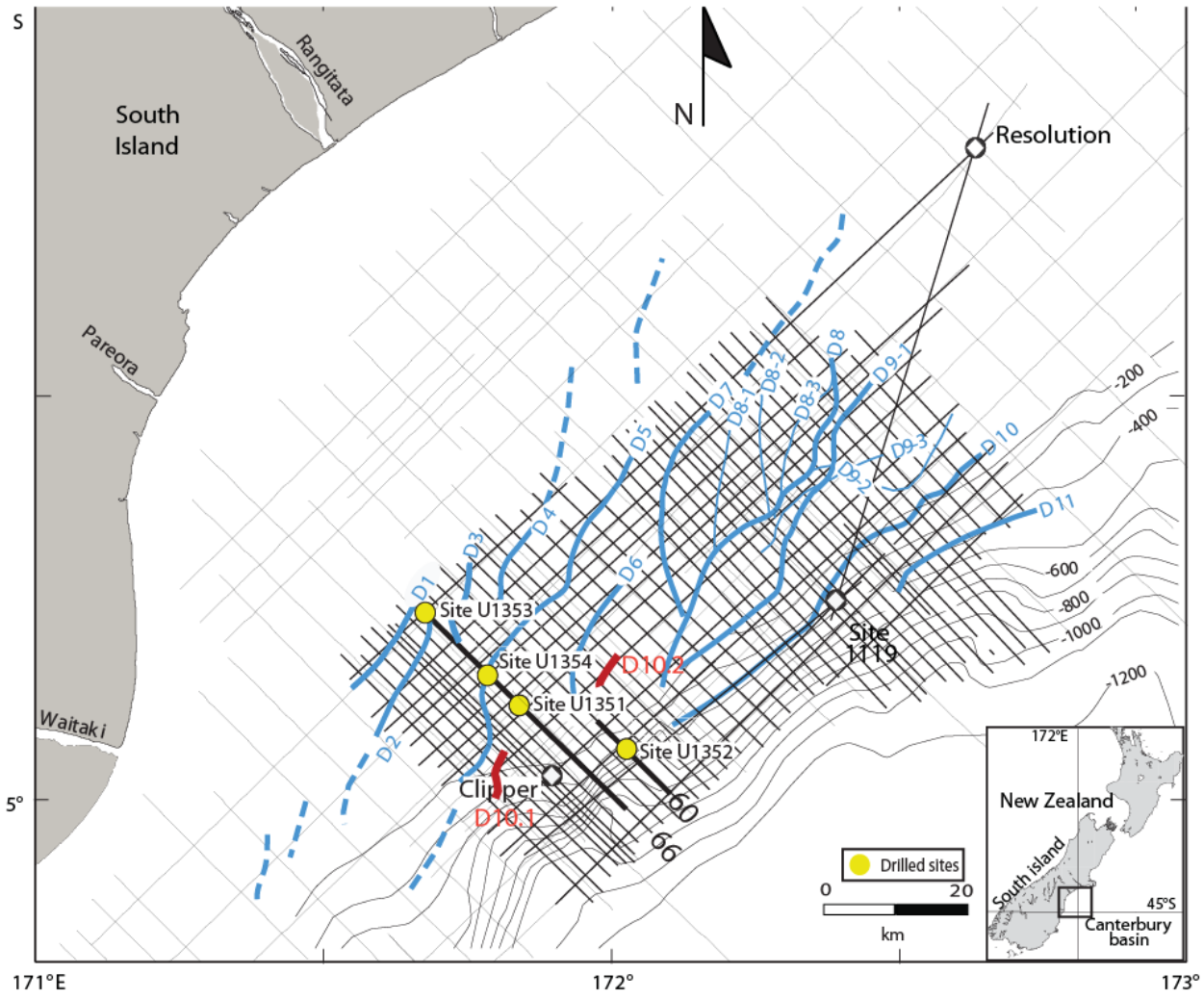

Figure 3.1: EW00-01 high resolution MCS grid (thick straight lines) and CB-82 low-resolution, commercial MCS (thin straight lines). Elongate sediment drifts (D1-D11) and two additional small scale drifts (D10.1 and D10.2: red lines) developed during the same period as D10, are also shown (curved lines mark the crests of drift mounds). Exploration wells, Clipper and Resolution together with ODP Site 1119 are also shown.

3.2 SEISMIC CHARACTERISTICS OF SEDIMENT DRIFTS AND WAVES

Analysis of 2-D MCS high resolution seismic data has revealed two additional contourite drifts (drifts D10.1 and D10.2), located in the southwestern part of the study area (Figures 3.1, 3.3 and 3.4). These features have also presumably been influenced by the northeastward flowing Southland Current (Figures 1.1 and 2.8). Sediment drifts and their associated facies, seismic characteristics, accumulation rates and classification have been described in detailed by McCave and Tucholke (1986), Eiken and Heinz (1993), Mèzerais et al. (1993), Carter and McCave (1994), Howe et al. (1994), Stoker et al. (1998), Faugères et al. (1999), and Stow et al. (2002, see their Fig. 4). Classification of sediment drifts is based on their external and internal geometries (Stow et al., 2002) used three scales of observation to classify the seismic characteristics of sediment drifts. Large-scale, first-order seismic elements include overall geometric architecture, orientation or direction of elongation, erosional discontinuities and reflection pattern (Figure 3.2). Based on such large-scale criteria, drifts can typically be classified as mounded, elongate or sheeted shapes and constrained by upper and lower boundaries (Figure 3.2). The elongation direction is usually oriented down-current. Uniform reflection patterns of moderate to low amplitude reflections are typical and indicate persistent stable conditions (Faugeres et al, 1999; Stow et al., 2002). Medium-scale seismic elements include internal seismic units, migration direction and reflection terminations. Most sediment drifts have lens-shaped, mounded (upwardly-convex) cross-sectional geometries (Figure 3.2). Internal progradational stacking patterns commonly imply migration in the down-current elongation direction. In most cases, drift internal reflections display downlapping terminations and sigmoidal progradational reflection patterns (Stow et al., 2002).

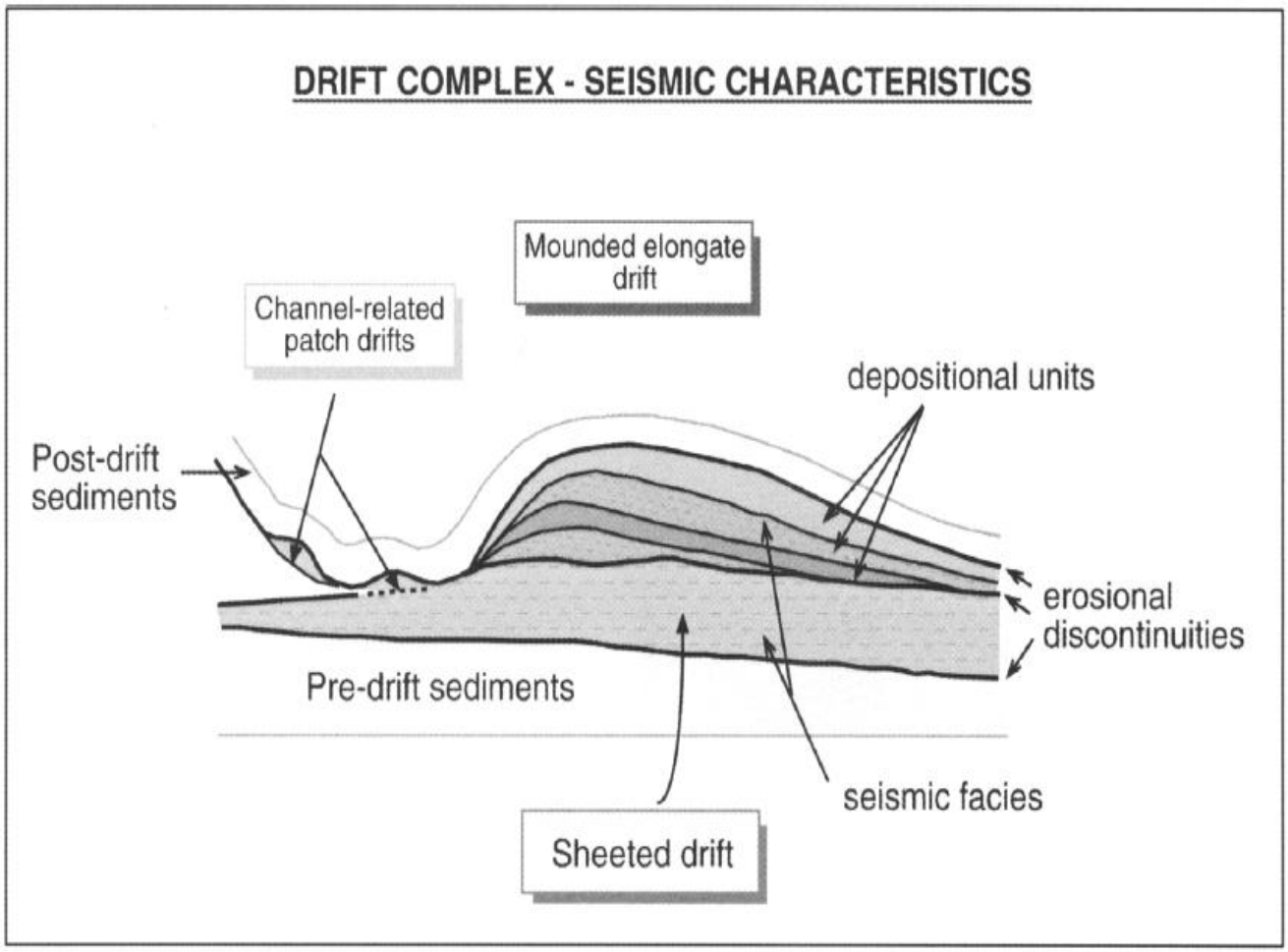

Figure 3.2: The schematic diagram of seismic characteristic of drift complex, including channel-related, mounded elongate, sheeted drifts (Stow et al., 2002).

At the smallest scale are third-order seismic elements based on seismic facies. The presences of continuous, sub-parallel reflections or wavy and irregular reflections are the most significant seismic facies that distinguish sediment drifts from sediments deposited by downslope processes (Stow et al., 2002). Drifts D10.1 and 10.2 are defined and mapped as plastered slope drifts that are located beneath the modern shelf-break in the southeastern part of the study area. They appear similar to sediment drifts as described that Stoker et al. (1998 and 2002) and Howe et al. (1994) in the northeastern Rockall Trough.

3.2.1 Slope Plastered Drifts`

Plastered drift D10.1 has low relief and is up to 151 m thick (Figure 3.3b). Mounded geometries and a distinct moat are not as well developed as in elongate drifts (Figure 3.3a). Internal reflections are dominantly continuous and relatively flat-lying. In addition, low-amplitude to transparent seismic facies and discontinuous reflections are present. In particular, some low-amplitude wavy reflections appear on the downslope flank of the drift (Figures.3.3a and 3.3b). Internal reflections onlap the paleoslope landward and downlap basinward. Drift D10.1 can be traced for 6 km along strike (Figure 3.3c).

D10.2 is located between D10.1 and D10 (Figure 3.1) and is also interpreted as a small scale plastered drift. However, it has a more distinctive mounded geometry, moat and its top is more incised by channel-like features than is D10.1 (Figures 3.4a and 3.4b). The moat separates the drift from the paleo-slope and the drift migrated upslope. The drift is up to 228 ms (~220 m) thick (Figure 3.4a) and is asymmetric in along-strike direction with ~16 km in width (Figures 3.1 and 3.4c). Internal reflection character also differs from D10.1. Internal reflections are dominantly discontinuous with onlap at the landward end of the drift. Seismic amplitudes are of medium intensity towards

downslope flank of the drift (Figures 3.4a and 3.4b). Both drifts D10.1 and D10.2 lie above sequence boundary U6 (10.4 Ma) and below U7 (9 Ma). Large, elongate drift D10, located in the northern part of the EW-0001 survey area, was also initiated above U6 and was active during deposition of drifts D10.1 and D10.2. However, it is important to recognize that the U6-U7 sequence was not generated entirely by current-related processes and other sedimentary processes were also active.

3.2.2 Sediment Waves

A large field of sediment waves is also observed beneath modern shelf break and slope, on mid- and lower paleoslopes, near the Expedition 317 sites (Figure 3.5). Small waves also occur on the upslope and down-slope flanks of drift D10.2 (Figures 3.4a and 3.4b). This large field of sediment waves is bounded below by seismic sequence boundary ~U13 (2.35 Ma) and above by seismic sequence boundary ~U16 (1.05 Ma). The internal seismic configuration of the waves comprises alternating low and high-amplitude reflections and climbing sinusoidal geometries within the upslope flank of the sediment waves (Figure 3.5). In contrast to the moderate-amplitude sinuous reflections within sediment waves on the lower slope, they feature less sinuous, parallel and sub-parallel reflections on upper paleoslopes (Figure 3.5). Wavelength varies from landward to basinward in response to increasing water depth, ranging from 0.5 km to 3 km (wavelength), and the deeper-water sediment waves are more symmetrical than those to landward (Figure 3.5). This sediment wave field indicates that current processes did not cease entirely in the southwestern part of the survey area in the Late Miocene (U7 time), but remained important contributors to deposition into the late Pliocene-early Pleistocene (~U13-U16 time).

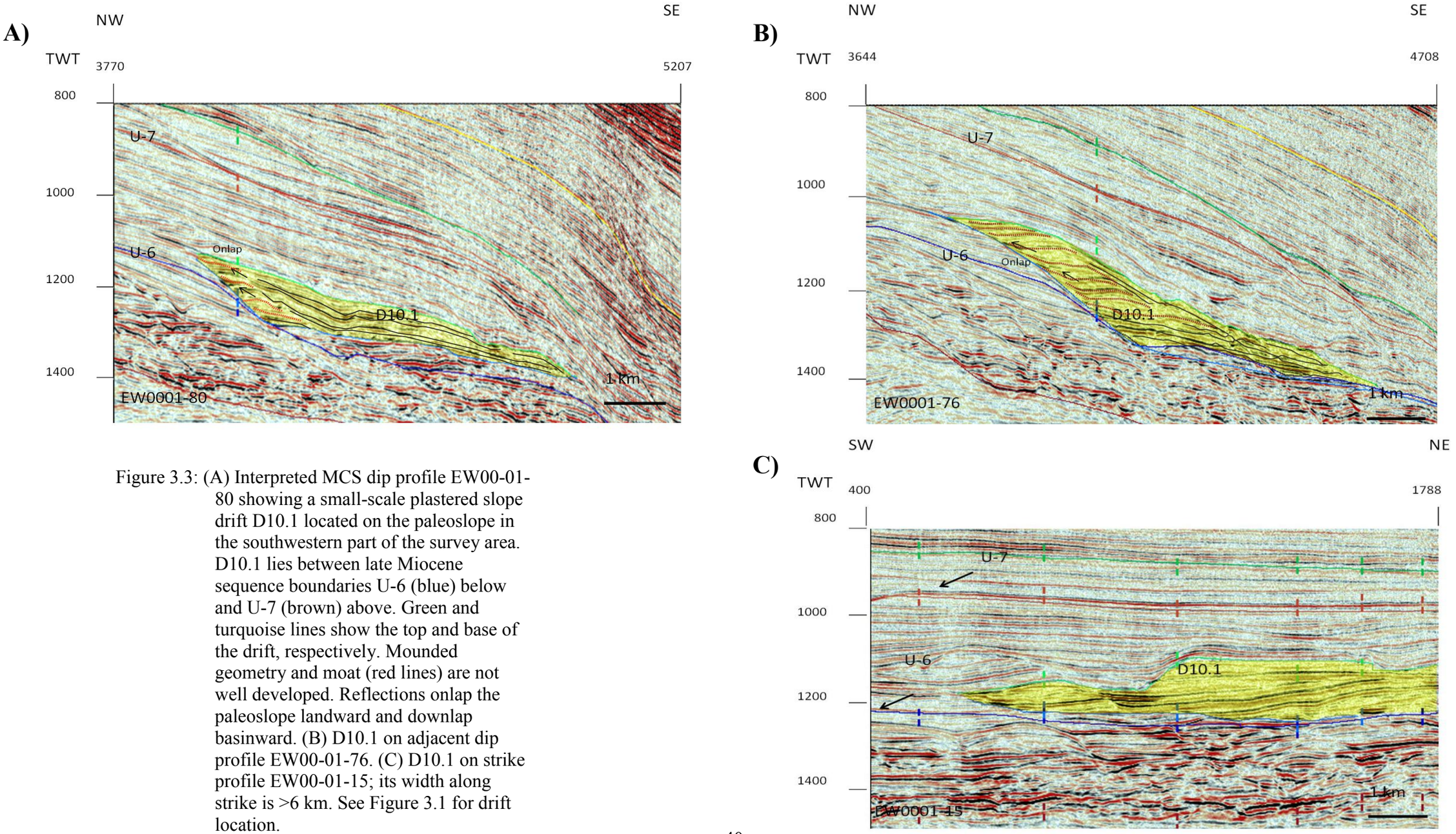

Figure 3.3: (A) Interpreted MCS dip profile EW00-01-80 showing a small-scale plastered slope drift D10.1 located on the paleoslope in the southwestern part of the survey area. D10.1 lies between late Miocene sequence boundaries U-6 (blue) below and U-7 (brown) above. Green and turquoise lines show the top and base of the drift, respectively. Mounded geometry and moat (red lines) are not well developed. Reflections onlap the paleoslope landward and downlap basinward. (B) D10.1 on adjacent dip profile EW00-01-76. (C) D10.1 on strike profile EW00-01-15; its width along strike is >6 km. See Figure 3.1 for drift location.

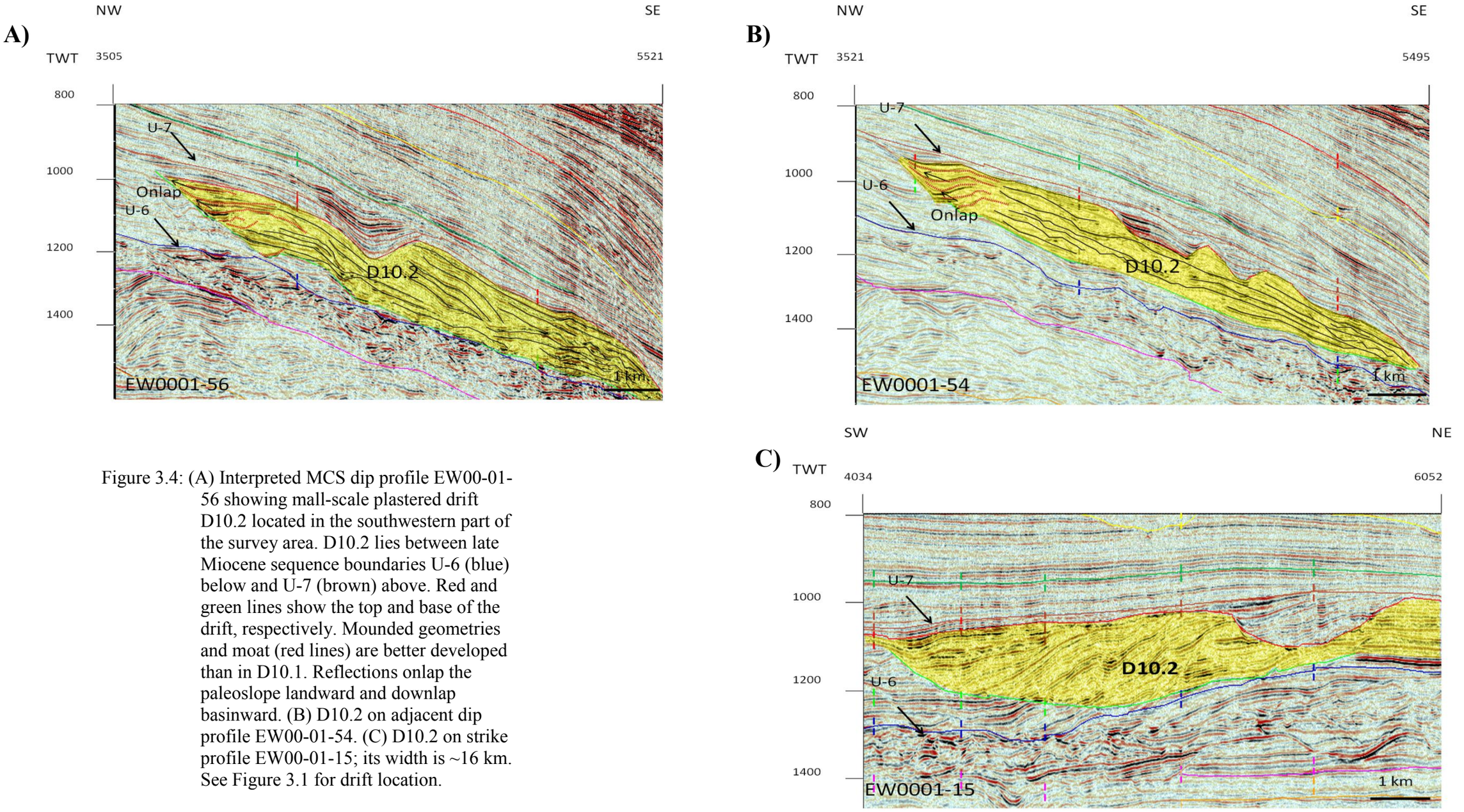

Figure 3.4: (A) Interpreted MCS dip profile EW00-01-56 showing mall-scale plastered drift D10.2 located in the southwestern part of the survey area. D10.2 lies between late Miocene sequence boundaries U-6 (blue) below and U-7 (brown) above. Red and green lines show the top and base of the drift, respectively. Mounded geometries and moat (red lines) are better developed than in D10.1. Reflections onlap the paleoslope landward and downlap basinward. (B) D10.2 on adjacent dip profile EW00-01-54. (C) D10.2 on strike profile EW00-01-15; its width is ~16 km. See Figure 3.1 for drift location.

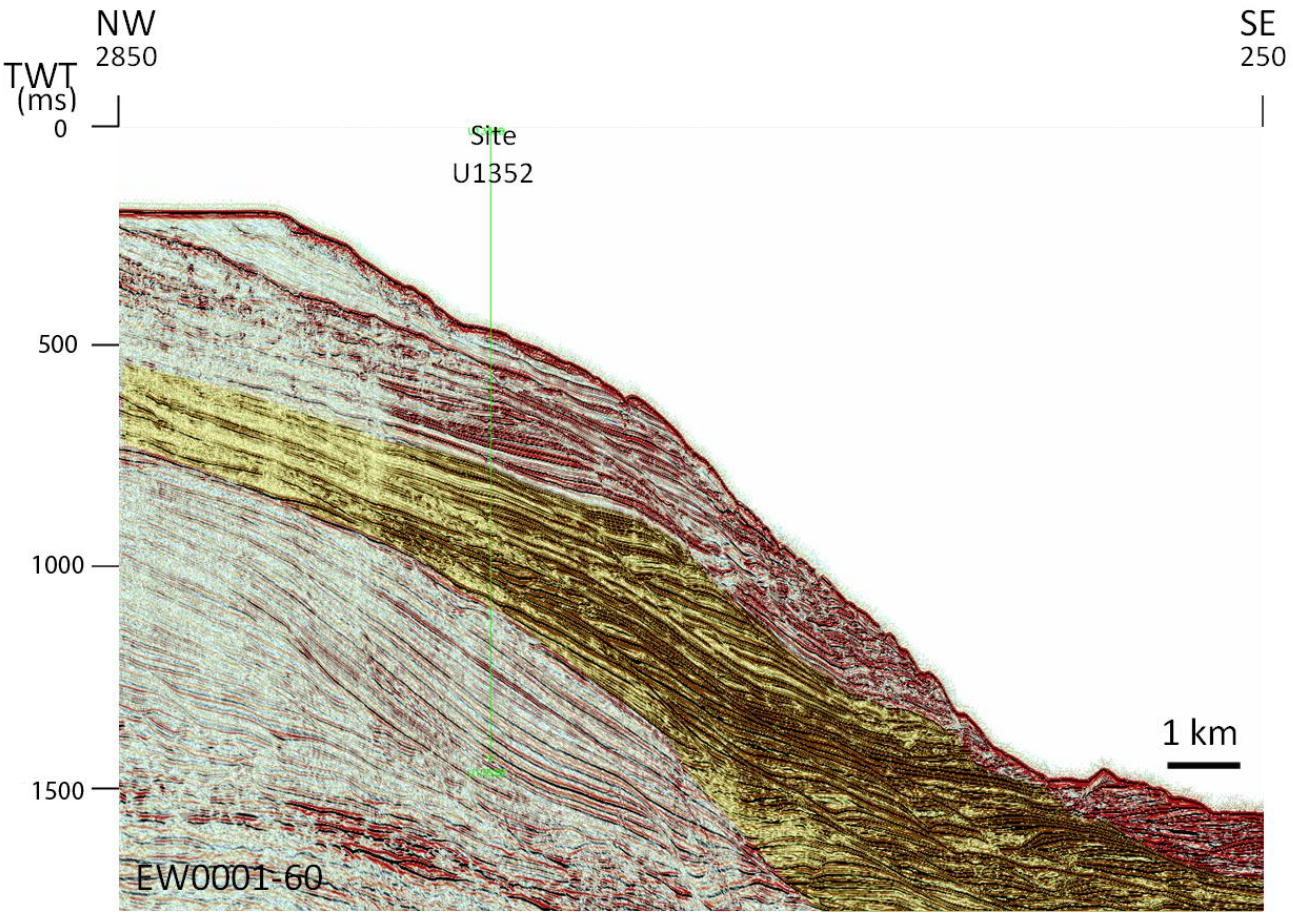

Figure 3.5: MCS dip profile EW00-01-60 showing large field of sediment waves (yellow shaded area) around IODP Site U1352. The sediment waves are characterized by moderate amplitude, variably sinuous, parallel and sub-parallel reflections on the lower and upper paleoslope. The shaded area is bounded below by seismic sequence boundary ~U13 (2.35 Ma) and above by seismic sequence boundary ~U16 (1.05 Ma). See Figure 3.1 for location.

3.2.3 Seismic and Core Evidence of Bottom Current Activity

Current controlled sediment accumulations resulted in sediment drifts and field of sediment waves on the mid-and upper slopes of continental margin (Imbert, & Viana, 1999; Faugères & Stow, 2008). Plastered sediment drifts (D10.1 and D10.2) controlled by the current processes were formed on the upper slope. These plastered drifts were initiated during the late Miocene in the southwestern part of study area. Both D10.1 and D10.2 lie between underlying sequence boundary U6 (10.4 Ma) and U7 (9 Ma) (Figure 3.3 and 3.4). These sequence boundaries were defined based on seismic termination (e.g., onlap, toplap, downlap and truncation) by Lu and Fulthorpe, (2004). The best seismic indicators of the Canterbury plastered drifts (1) low-relief accumulation in the paleo-slope setting; (2) convex-upward mounded geometries; (3) continuous flat-lying, discontinuous and wavy internal reflections; (4) downlapping and onlapping reflectors (Figure 3.3 and 3.4). However, other sedimentary processes, particularly sediment transport, were also be active on the margin. Therefore, the sequences were not generated entirely by current-related processes. For example, channel incisions in the upper surfaces of drifts indicate that downslope processes influenced drift development and sequence evolution (Figure 3.4b). In addition, sediment waves can develop on the slope, particularly on the lower slope and at slope toe (Figure 3.5). IODP Expedition 317 Site U1352 lies on the upper slope (344 m water depth) on dip profile EW00-01-60 (Figure 2.10 B) provide information about the principal facies forming the sediment waves in the shaded area on Figure 3.5. The shaded area is bounded below by seismic sequence boundary ~U13 (2.35 Ma) and above by seismic sequence boundary ~U16 (1.05 Ma) (equivalent to 490 m below and above 246 m). The general facies are fine-grained, mud-rich sediment with interbedded decimeter-centimeter thick sand and sandy mud. Sediment properties within the interval of sediment waves are (1) poorly developed

sedimentary structures or structureless; (2) sharp upper and lower contact between mud and sand; (3) rhythmic decimeter to centimeter sand and mud; (Figure 3.6). These observations are consistent with deposition as contourites under the influence of currents. Similar characteristic features for current-related sediment waves were proposed by Ediger et al. (2002) in the Cilician Basin. Sharp upper contacts at the tops of sand layers are considered particularly strong evidence for current activity when the contact is not erosional (Shanmugam et al. 1993).

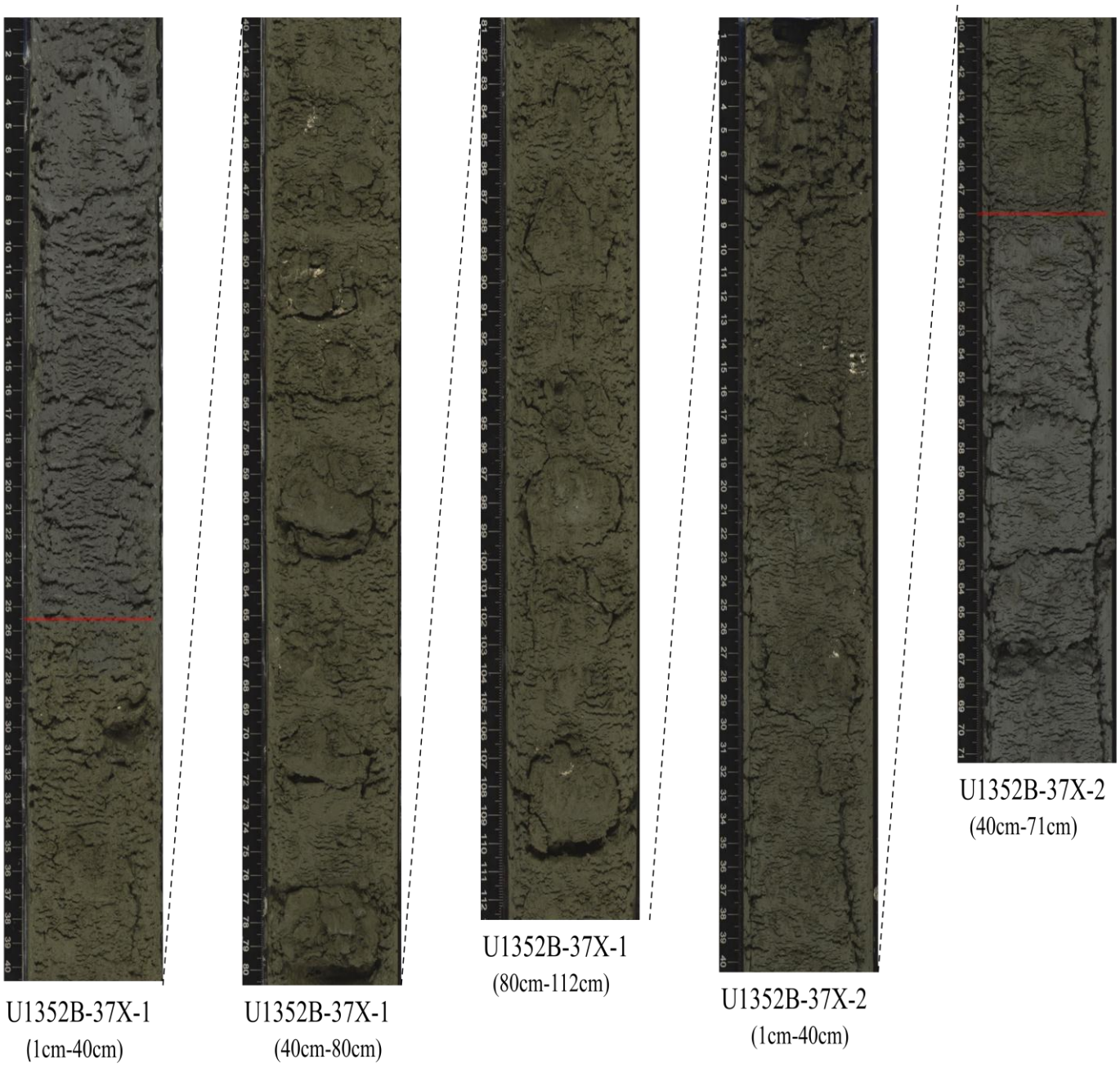

Figure 3.6: Images from core sections U1351B-37X-1 and U1351B-37X-2 showing sharp upper and lower contacts (red lines) between greenish gray fine sand, with shell fragments and poor bedding, and homogenous mud. The sharp upper (26 cm in core section U1352B-37X-1) and lower (48 cm in core section U1352B-37X-2) contacts of the sand layer, together with the poor bedding, are evidence of traction surfaces created by bottom current activity.

CHAPTER 4: LITHOLOGIC EXPRESSION OF SEQUENCE BOUNDARIES BASED ON PREDICTED DEPTHS

4.1 INTRODUCTION

Correalation of seismically interpreted sequence boundaries with lithologic surfaces observed in cores from the Expedition 317 Sites contributes to understanding the origins and preservation of seismically resolvable sequences. Expedition 317 drilled Middle Miocene to Recent sequences at four sites: Sites U1351, U1352 and U1353 are located on the continental shelf and Site U1352 is located on the upper slope (Figure 2.9). Prior to drilling, nineteen regional seismic sequence boundaries (U19-U1) were interpreted using the EW00-01 seismic data by Lu and Fulthorpe, 2004. These sequence boundaries were interpreted based on seismic terminations (e.g., onlap, toplap, downlap and truncation) and were tentatively correlated with the eustatic chart of Haq et al. (1987) (Lu and Fulthorpe, 2004). The section was also divided two larger seismic units (Figures 4.1 and 4.2). The upper seismic unit (U19-U11) is downlapped on paleoshelves, where a number of channel incisions are observed, and shelf-edge rollovers are angular. Internal reflection geometries are oblique. In contrast, the lower seismic unit (U10-U5) features rounded shelf-edge rollovers with sigmoidal reflections pattern. Onlap is more common on paleoshelves and truncation less common.

Lithologic discontinuity surfaces and their associated sediment facies were identified in cores during Expedition 317 and tentatively correlated with sequence boundaries by shipboard scientists (Fulthorpe et al., 2011). I have reviewed these interpretations as part of this study using the shipboard core descriptions, emphasizing grain-size contrasts, the nature of the lower and upper contacts of the sediment packages and the predicted depths of seismically interpreted sequence boundaries derived from the

three approaches discussed in Chapter 2, e.g., the precruise time-depth function, Brusova (2010), and synthetic seismogram derived from holes U1351B and U1352B). Data from Sites U1353 and U1354 were not used for core-seismic correlation because of the limited of wireline log data available from those sites. Correlations between core lithologic surfaces and the predicted depths to seismically interpreted sequence boundaries provide insight into how well each of the three time/depth models perform for Sites U1351 and U1352.

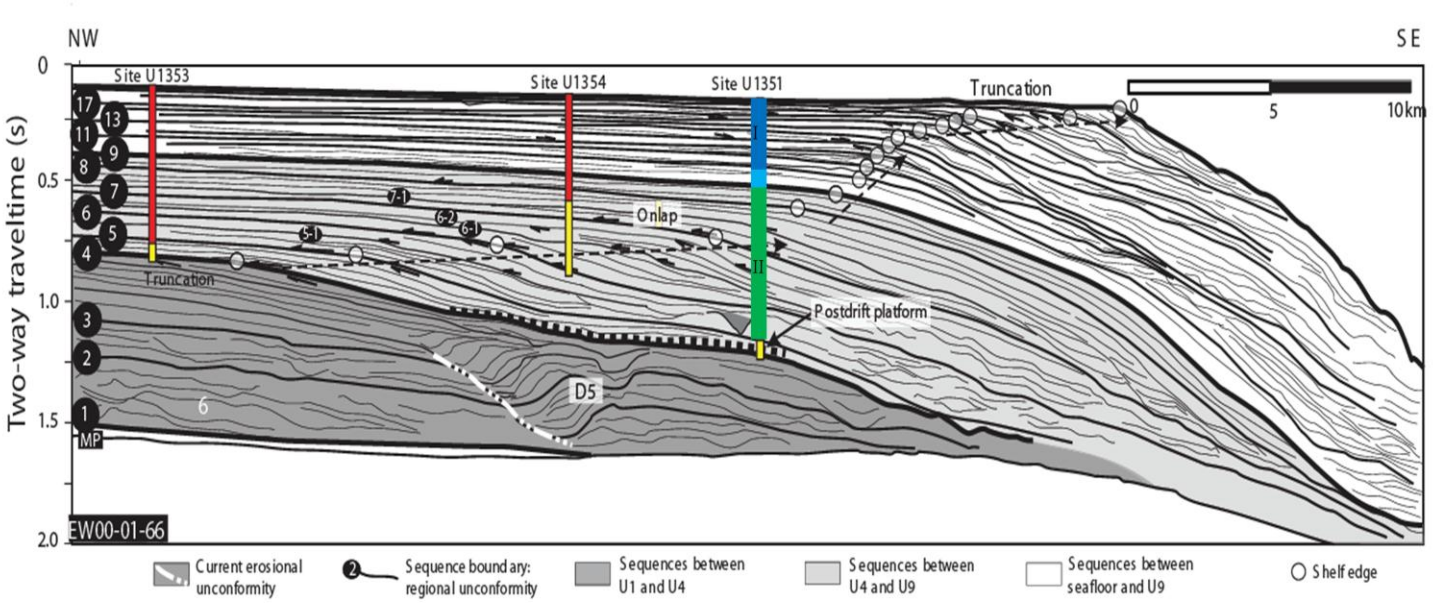

Figure 4.1: Interpreted MCS profile EW00-01-66 showing locations of Sites U1351, U1353 and U1354. Actual penetrations are show in red, planned penetrations in yellow. Expedition 317 lithostratigraphic units are also shown at Site U1351. Reflection termination and shelf-edge trajectory are also shown (Fulthorpe, et al., 2011). See Figure 3.3 for line location.

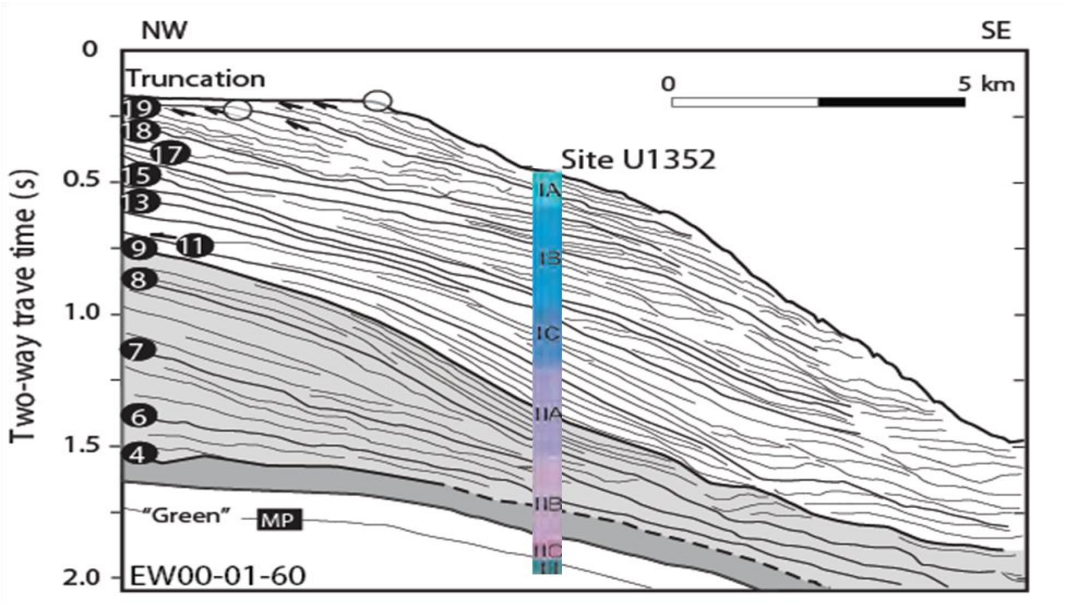

Figure 4.2: Interpreted MCS profile EW00-01-60 showing Expedition 317 lithostratigraphic units (Fulthorpe, et al., 2011). See Figure 3.3 for location.

4.2 SITES U1351 AND U1352 OVERVIEW

Site U1351 is situated on the outer shelf in a water depth of 122 m and overlain on dip seismic profile EW00-01-66 (Figures 2.10 A and 4.1). Three holes were drilled at this site (Holes U1351A, U1351B, and U1351C). Maximum penetration was 1030.6 m at Hole U1351B. The advanced piston corer (APC), extended core barrel (XCB) and rotary core barrel (RCB) were deployed in succession maximize recovery as cementation increased with depth. Total recovery varies with holes condition and penetration; IODP has historically found the unconsolidated cohesionless sediments that are common on continental margins difficult to recover. For example, Hole U1351A recovered 27.3 m of sediment corresponding to 98% of total penetration which was, however, only of 28 m. In contrast, Hole U1351B recovered 304.5 m corresponding to the 30% percent of its deeper total penetration of 1030.6 m. Hole U1351C was not cored because it was drilled only for wireline logging (Table 2.2). Site U1352 lies on the upper slope (344 m water depth) on dip profile EW00-01-60 (Figures 2.10 B and 4.2). Four holes were drilled at this site. Maximum penetration was 1927.5 m at Hole U1352C**.** Penetration and recovery information for all holes is provided in Table 2.2.

4.3 LITHOSTRATIGRAPHY OF SITE U1351 AND LITHOLOGIC EXPRESSION OF SEQUENCE BOUNDARIES

The general lithostratigraphy for Expedition 317 was first defined based on Hole U1351B at Site U1351, the first site to be drilled. Two fundamental lithologic units were identified based on lithologic composition by Expedetion 317 scientists (Fulthorpe et al., 2011). These units were also identified at each of the other three Expedition 317 sites. Lithostratigraphic Unit 1 (0-262 m) is composed of dark gray and dark greenish gray mud and sandy mud with intermittent centimeter to decimeter thick; well-sorted fine sand and abundant shell fragments. Heavy bioturbation is common but distinct bedding structures are rare. The lower part of Unit 1 contains greenish gray calcareous beds with less

bioturbation. Lithologic boundaries within the upper and middle parts of Unit 1 are sharp but, those within the lower part are more gradational.

In contrast, lithostratigraphic Unit 2 (262-1024.4 m) consists of more homogeneous facies than those of the Unit 1. Unit 2 is mainly composed of dark greenish gray mud and muddy sand with less abundant carbonate cementation. Some shell fragments are present at the top of the unit; bioturbation is decreased with depth. Lithologic surfaces are more gradational than in Unit 1, but few such sharp contacts are observed in Unit 2.

It is possible to attempt correlation of lithologic boundaries and associated sediment packages observed in Unit 1 to seismically resolvable sequence boundaries U12 and U19. However, low recovery near the predicted depths of seismically interpreted sequence boundaries in Unit 2, together with the more gradational lithologic boundaries characteristic of that unit, prevent core-seismic correlation of sequence boundaries (below U12). In addition, lack of appropriate wireline logs, particularly sonic and density logs limited out ability to determine predicted depths of seismic sequence boundaries below U12 using synthetic seismograms derived from sonic and density logs. Therefore, although Table 4.1 shows predicted depth of seismically resolvable sequence boundaries through the entire interval between U5 and U19, only sequence boundaries (U12-U19) could be correlated with lithologic surfaces observed in core derived from hole U1351B using depth predictions derived from all three techniques discussed in this study, i.e., precruise time/depth function, Brusova (2010), and synthetic seismograms (see Chapter 2). This study uses same numerical system for lithologic boundaries observed in cores (e.g., U1351B-S1) as used by Expedition 317 shipboard scientists (Fulthorpe et al., 2011).

U1351B-S1: The lithologic expression of this boundary is a sharp, burrowed basal contacts separating greenish gray shelly sandy mud above from the gray mud below. A concentration of shell fragments 30 cm thick above the contact. The boundary is located at a depth of 15.955 m below sea floor and observed in core section 317-U1351B-2H-6 (Figure 4.3). The U1351B-S1 contact is correlated with sequence boundary U19. The observed depth of the U1351B-S1 in core closest to the predicted depths U19 derived from the precuise and Brusova functions than to that derived using the synthetic seismogram (Table 4.1).

U1351B-S2: The boundary is represented by a sharp contact between dark greenish gray sandy mud above and very fine well sorted sand below. The boundary is located at the depth of 29.51 m below sea floor core section 317-U1351B-5H-1 (Figure 4.4) and it is ~ 1.5 m shallower from tentative placement by shipboard scientists during Expedition 317. This tentative placement of the surface S2 is located at top of the core in U1351B-5H-3, at 3 cm, separating very fine sand from underlying greenish gray sandy mud, therefore; this sand might be thought a result of downhole caving. In addition, the U1351B-S2 boundary is correlated with the seismic sequence boundary U18. The observed depth of the U1351B-S2 in core is closest to the Brusova (2010) sequence boundary depth prediction for U18 (Table 4.1). The synthetic and precruise depth predictions for U18 are poorer fits.

Table 4.1: Predicted depths of seismically resolvable sequence boundaries at Hole U1351B based on the precruise time/depth function, Brusova (2010) and synthetic seismogram compared to depths of correlative lithologic surfaces observed sequence boundaries in cores.

Sequence Boundary	TWT (s) BSF	Precruise function depth (m)	Brusova function depth (m)	Synthetic depth (m)	Observed sequnce boundary from core (m)
U1351B-19	0.0205	16.1	16.1	15.3	15.955
U1351B-18	0.0375	28.9	29.6	33.1	29.51
U1351B-17	0.063	49	50.1	54.1	52.26
U1351B-16	0.08	62.7	63.9	67.8	70.33
U1351B-15	0.106	83.9	85.2	90.2	88.86
U1351B-14	0.127	101.4	102.6	107.9	no core
U1351B-13	0.1635	132.5	133.4	138.7	144.13
U1351B-12	0.2015	163.9	166	168.3	171.42
U1351B-11	0.232	193	192.8	195.8	no core
U1351B-10	0.278	235.3	234	235.7	
U1351B-9	0.3555	309.7	305.5	307.5	
U1351B-8	0.437	391.9	384.3	386.5	
U1351B-7	0.638	612.9	592.9	582.7	
U1351B-6	0.865	893.1	851	804.8	
U1351B-5	0.997	1071.2	1008.5	933.9	

Figure 4.3: Core section U1351B-2H-6 showing lithological boundary U1351B-S1 at 15.955 m. The sharp basal contact separates ~80 cm shelly sandy mud from underlying gray mud. The mud beneath the contact is heavily burrowed, with burrows extendings up to 60 cm beneath the contact. This contact is correlated with seismically interpreted sequence boundary U19.

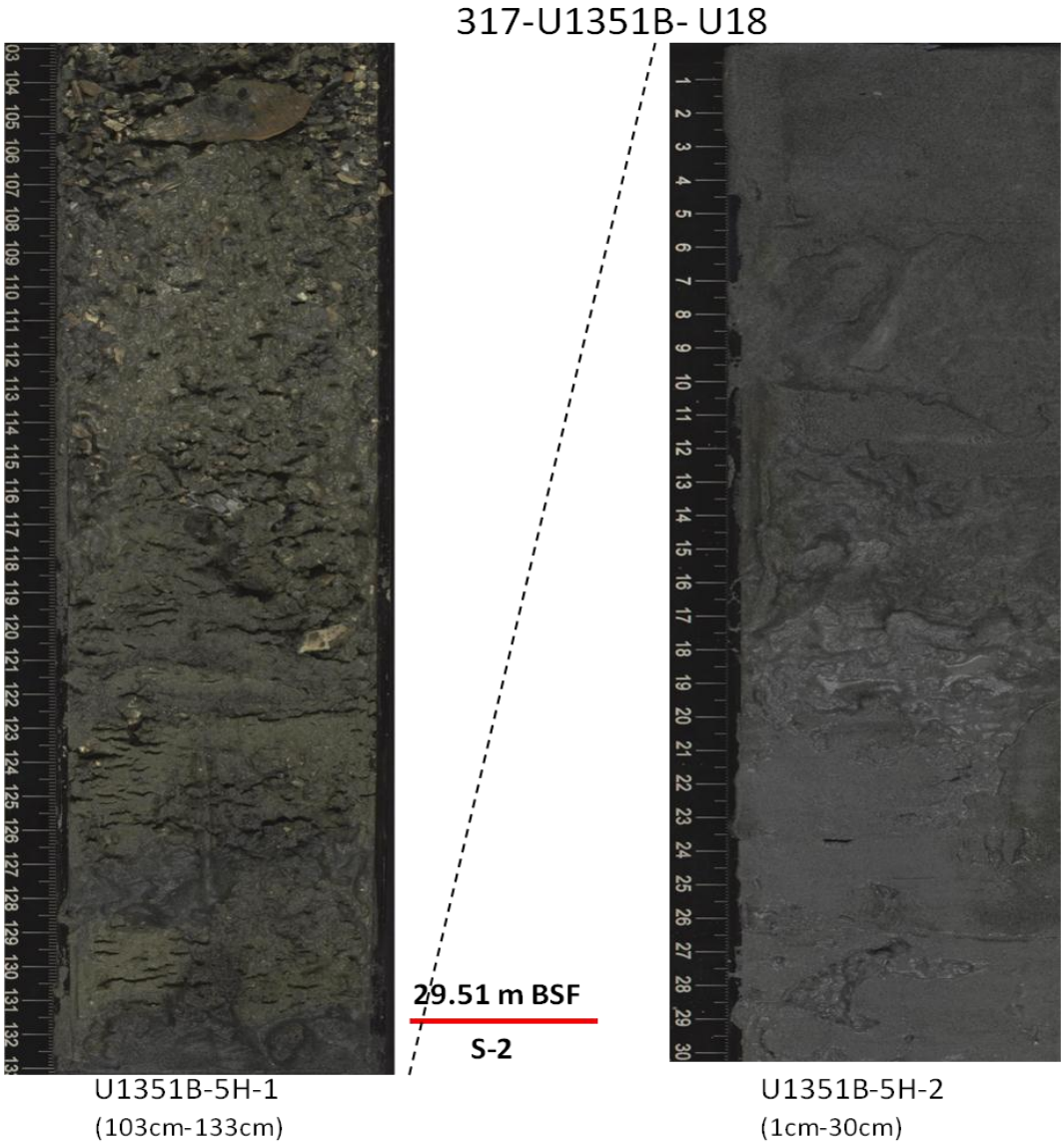

Figure 4.4: Core section U1351B-5H-1 showing lithologic surface U1351B-S2 at 29.51 m. A sharp contact separates dark greenish gray sandy mud with the common shell fragments from underlying very fine well sorted thick shelly sand. This contact is correlated the seismically interpreted sequence boundary U18.

U1351B-S3: This boundary is a sharp basal contact separating 15 cm thick medium coarse sand above from silt below. The upper part of the contact is extremely bioturbated, but below the contact is represented by centimeter-diameter burrows infilled with greenish mud. The boundary is occurs in core section 317-U1351B-8H-4 at 52.26 m below sea floor (Figure 4.5) and is correlated with seismic sequence boundary U17. Both the Brusova and synthetic depth predictions for U17 are close to the observed depth of U1351B-S3 in core (Table 4.1).

U1351B-S4: The U1351B-S4 boundary represented by a sharp erosional basal contact. This contact is placed (~3 m deeper than the shipboard tentative placement) at depth of 70.33 m in section 317-U1351B-11H-1 at 64cm (Figure 4.6) because shelly sand overlying on the top of the tentative placement might be considered downhole caving sand. It separates greenish shelly sandy mud above from gray homogeneous mud below. Heavy burrowing and concentration of shell fragments appear in above the contact extends up to 64 cm above the contact (Figure 4.6). The Brusova (2010) and precruise functions predict the depth of sequence boundary U16 ~6-7 m below U1351B-S4 (Table 4.1). However, the synthetic provided a closer depth prediction for U16, differing by only ~2.5 m from the depth of U1351B-S4 (Table 4.1).

U1351B-S5: At U1351B-S5, a sharp erosional contact separates dark gray well sorted sand above from dark grey mud with ~5 cm thick light grey clay beds below (Figure 4.7). I chose that surface as the sequence boundary at depth of 88.86 m in core section 317-U1351B-1H-3 at 118 cm because it is ~12 m deeper than the tentative shipboard placement and it is closer to the predicted depth of seismic sequence boundary U15. It is correlated with the seismic sequence boundary U15. The depth of U1351B-S5 in core is close to the predicted depth of U15 (90.2 m) derived from the synthetic (Table 4.1).

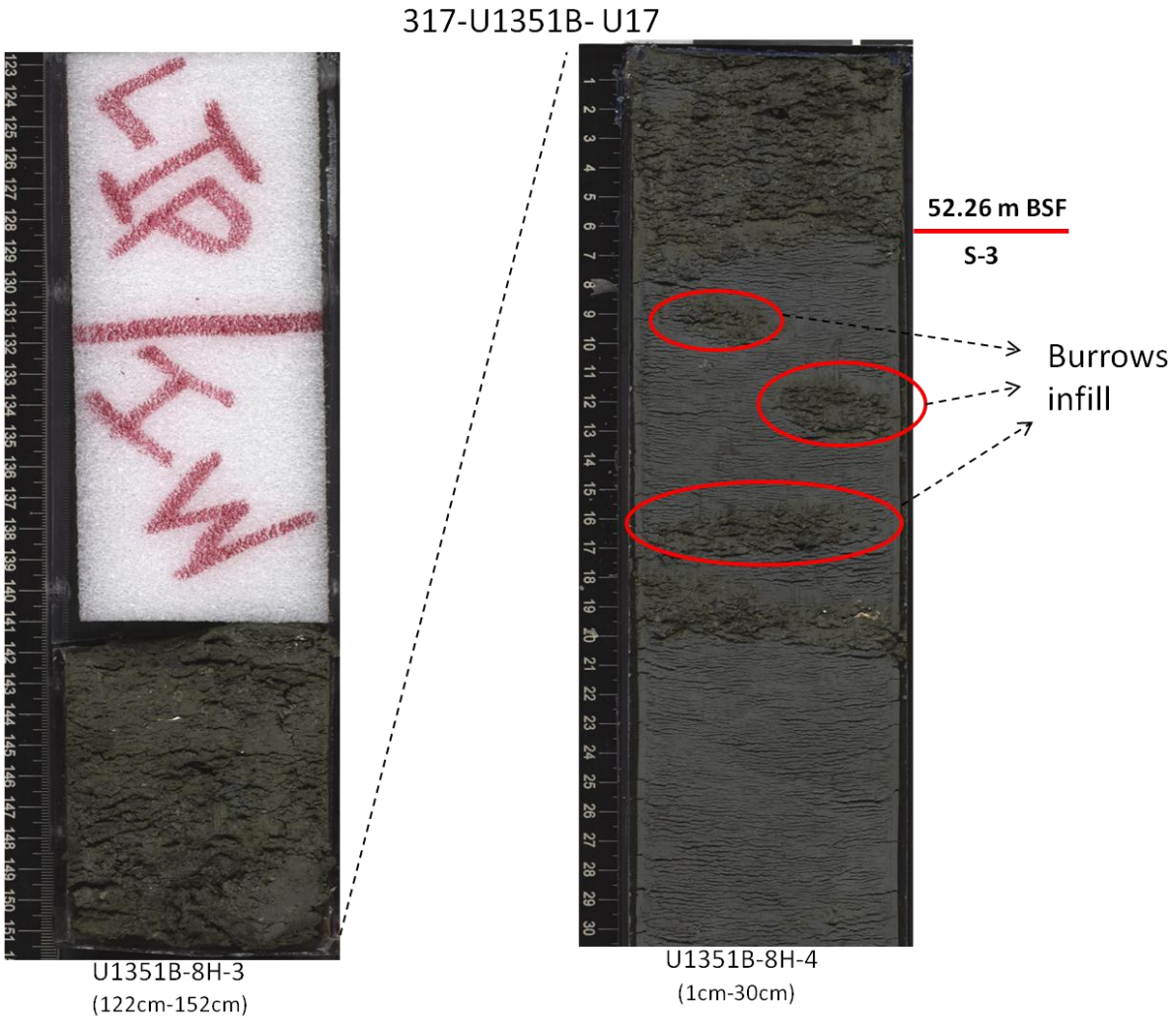

Figure 4.5: Images from core sections U1351B-8H-3 and U1351B-8H-4 showing lithologic boundary U1351B-S3 as a sharp basal contact at 52.26 m separating 15 cm thick fine to medium coarse sand from underlying silt with intense burrowing (red ellipses indicate burrow fill). Burrows extend up to 15 cm below the contact and the fills contain rare shell fragments. This contact is correlated with seismically interpreted sequence boundary U17.

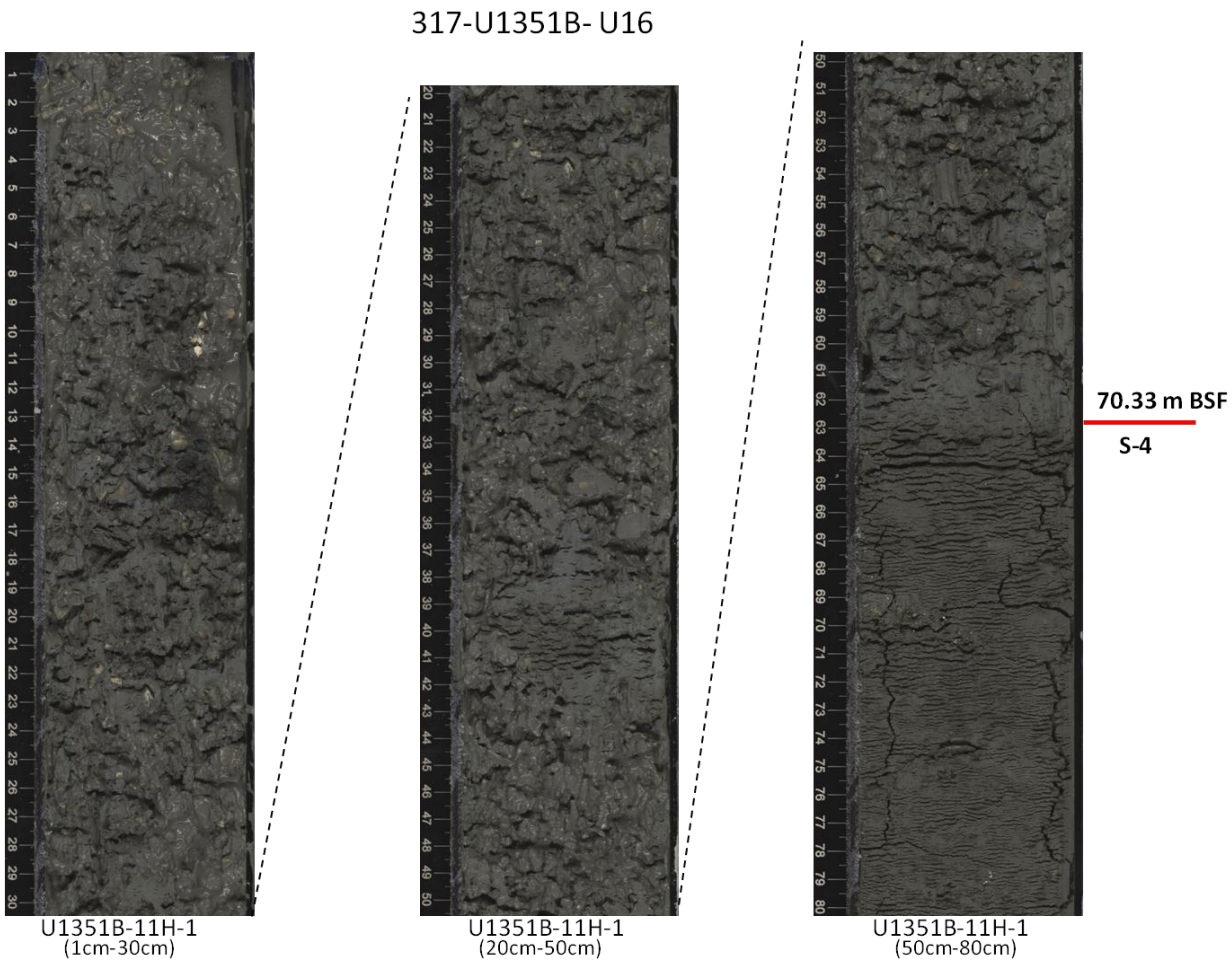

Figure 4.6: Core section U1351B-11H-1 showing lithologic boundary U1351B-S4 as a sharp basal contact at 70.33 m separating greenish shelly fine sand from underlying dark grey mud. This contact is correlated with the seismic sequence boundary U16.

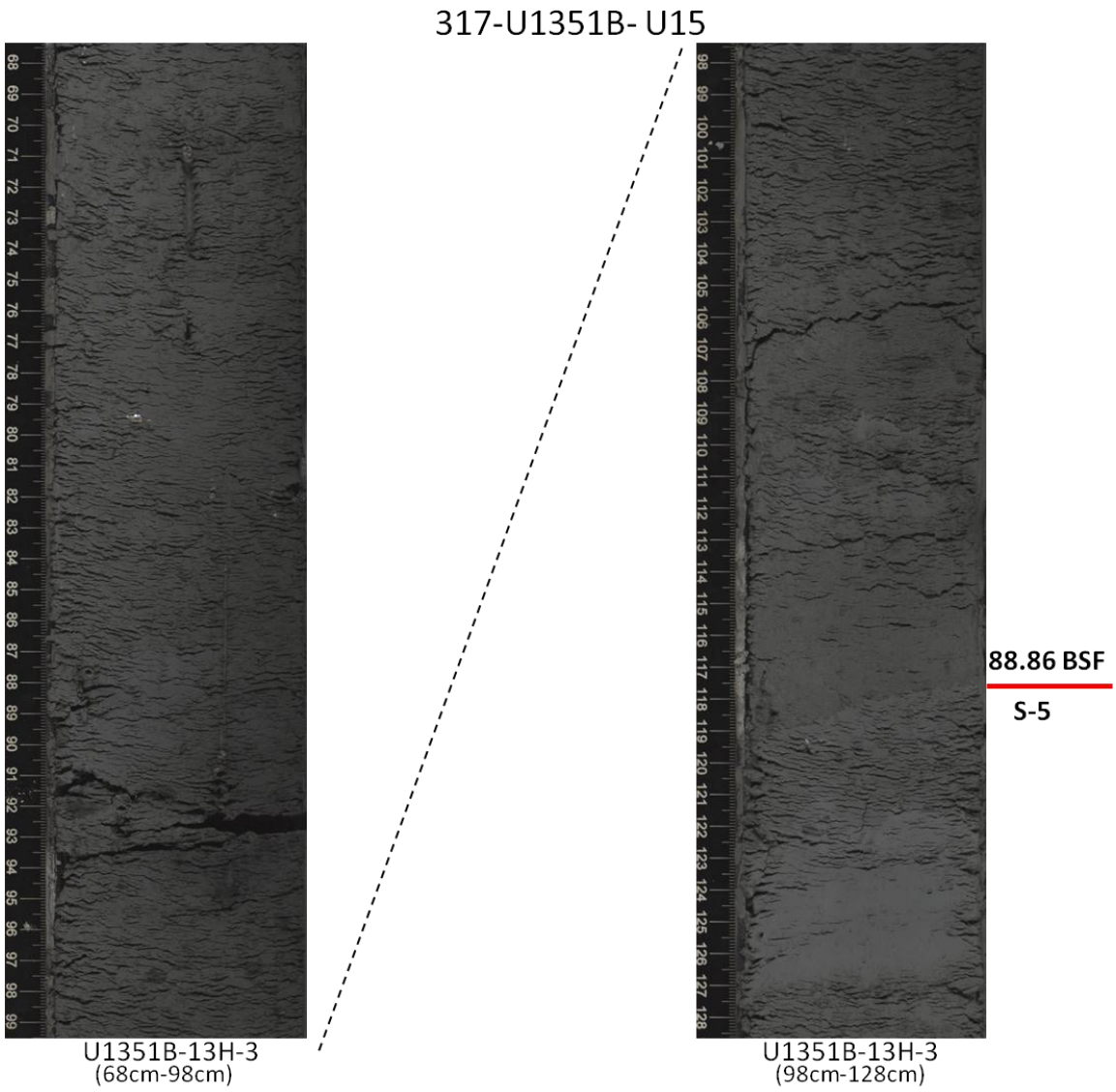

Figure 4.7: Core image section U1351B-13H-3 showing lithologic contact U1351B-S5 as a sharp basal contact at 88.86 m separating dark grey well-sorted sand from underlying dark grey mud with interbedded centimeter-thick light grey clays. This contact is correlated with seismic sequence boundary U15.

U1351B-S6: This boundary is represented by a sharp basal contact between very fine shelly sand above and gray shelly mud below. U1351B-S6 lies at a depth of 144.13 m in the section 317-U1351B-19X-2 at 104cm (Figure 4.8). It is correlated with the seismically interpreted sequence boundary U13. The synthetic seismogram provides the closest correlation (138.7 m) between depths of U1351B-S6 and U13, but the predicted depth of U13 is still over 5m shallower than the depth to the litholigical contact.

U1351B-S7 This boundary consists of a sharp erosional contact separating dark greenish gray very fine sand and shelly mud above from dark grey clayey mud below (Figure 4.9). Burrows extend up to 25 cm below the contact and are infilled with the greenish gray sandy mud from above the contact (Figure 4.9). The U1351B-S7 contact is close to the predicted depth of seismic sequence boundary U12. Once again, the synthetic yields the closest correlation between the predicted depth of U12 (168.3 m) and the depth of U1351B-S7 in core (171.42 m) (Table 4.1).

Figure 4.8: Core section U1351B-19X-2 showing lithologic boundary U1351B-S6 as a sharp basal contact at 144.13 m separating very fine shelly sand from underlying grey shelly mud with infilled burrows. This contact is correlated with the seismic sequence boundary U13.

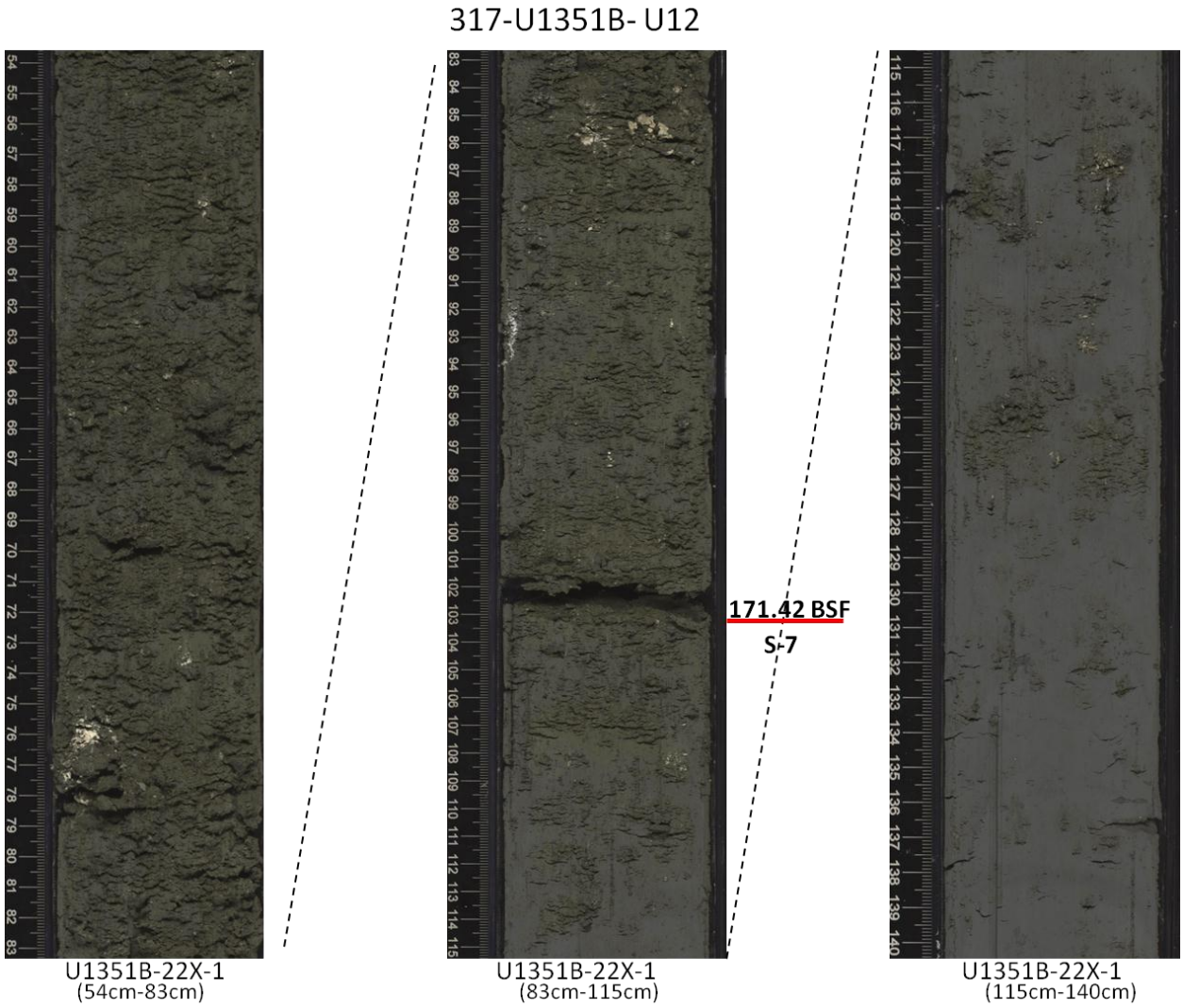

Figure 4.9: Core section U1351B-12X-1 showing lithologic boundary U1351B-S7 as a sharp burrowed basal contact at 171.42 m separating dark greenish gray very fine sand and shelly mud from underlying dark grey clayey mud. Infilled burrows extend up to 25 cm below the contact. This contact is correlated with seismic sequence boundary U12.

4.4 LITHOSTRATIGRAPHY OF SITE U1352 AND LITHOLOGIC EXPRESSION OF SEQUENCE BOUNDARIES

Lithostratigraphy at Site U1352 follows the same general pattern as at Site U1351, but a third lithological unit was added reflecting the greater penetration at Site U1352 and slope location of the site (Fulthorpe et al., 2011). Lithostratigraphic Unit 1 (0-710 m) contains mud-rich sediment. The mud contains interbeds, a few centimeters thick, of very fine to fine muddy sand, sandy mud and, sand within the upper 100 m. Between 100 m and 450 m the lithology comprises calcareous sandy mud, mud, clay and rare shell fragments. At approximately 450 m is a transition from mud-rich sediment to carbonate-rich sediment in response to the downhole change paleodepth from shallower to deeper slope environments. Observed lithologic boundaries are mostly sharp, but some gradational boundaries also appear within the Unit 1.

Lithostratigraphic Unit 2 (710-1853 m) is dominated by slope deposits containing calcareous mud, sandy mud, marlstone and chalk. A transition from marlstone to limestone occurs in the lower part of Unit 2 at ~1700 m.

Unit-3 (1853-1924 m) is clean foraminiferal limestone and was recovered from the deepest sediment hole U1352C ever drilled by IODP.

Based on the lithologic description at Site U1352, lithologic boundaries and associated sediment packages from Unit 1 were integrated empirically with seismically resolvable sequence boundaries U14 and U19, using the predicted depths of seismically interpreted sequence boundaries derived from precruise function, Brusova (2010), and the synthetic seismogram for U1352B (Table 4.2). Deeper seismic sequence boundaries (U4-U13) could not be correlated to the cores because of gradational nature of the deeper contacts, particularly in this slope settings, and limitations in recovery and depth achieved by logging. Once again, this study uses the same numerical system for lithologic

boundaries observed in cores (e.g., U1352B-S1) as used by Expedition 317 shipboard scientists (Fulthorpe, et al., 2011).

U1352B-S1: This boundary is a sharp contact separating thick, >1 m, dark greenish gray fine to medium calcareous sand above from dark greenish gray mud below. The contact is at depth of 62.15 m below sea floor in section 317-U1352B-7H-6 at 94 cm (Figure 4.10). Concentrations of shell fragments are present above and below the boundary. In addition, centimeter-scale burrows, infilled with greenish gray mud, are observed below the contact (Figure 4.10). This contact lies near the predicted depth of seismic sequence boundary U19 and is assumed to be correlative with the U19. However, the U1352B-S1 surface observed in core is approximately 6 m shallower than the predicted depth of U19 based on the precruise and Brusova (2010) time/depth functions and over 10 m shallower that the depth predicted using the synthetic (Table 4.2).

U1352B-S2: The U1352B-S2 boundary is also a contact separating overlying greenish gray muddy sand with scattered shell fragments from underlying dark gray to greenish gray mud. This burrowed contact is observed at depth of 147.22 m below sea floor in section 317-U1352B-16H-5 at 5 cm (Figure 4.11). The discrete burrows occurrs below the contact and calcareous concretion appears in between 129 and 134 cm from the section top in 317-U1352B-16H-4 (Figure 4.11). The boundary lies near the predicted depth of seismic sequence boundary U18. Although U1352B-S2 is the best candidate surface to correlate with U18 the closest predicted depth for U18, derived from the synthetic, is approximately 3 m deeper than U1352B-S-2 in core.

U1352B-S3: This boundary is located at 207.04 m below sea floor in core section 317-U1352B-23H-6, at 84 cm, where the burrowed contact separates overlying ~ 1 thick, dark greenish muddy sand bed with rare shell fragment from underlying gray mud. Burrows sand extend up to 23 cm below the contact (Figure 4.12). This contact is

observed near the predicted depth of seismic sequence boundary U17. The U1352B-S3 surface is the best candidate surface for correlation with U17, but the closest predicted depth for U17 derived from the synthetic, is approximately 10 m shallower than that of the surface in core.

U1352B-S4: This boundary is similar to the U1352-S3 boundary. Both boundaries separate overlying bioturbated dark greenish muddy sand from underlying burrowed gray mud. The sand-filled burrows extend up to 40 cm below the contact, which is observed at a depth of 246.59 m below sea floor in section 317-U1352B-28H-1, at 40 cm (Figure 4.13). This boundary lies on near the predicted depth of seismic sequence boundary U16. This boundary is also ~3.5 m shallower than the tentative shipboard placement because it is more distinguishable in cored interval; the synthetic yields the closest correlation between U16 and U1352-S4 (within ~1.5 m), but the precruise and Brisova functions are also close (within 2 m; Table 4.2).

Table 4.2: Predicted depths of seismically resolvable sequence boundaries at Hole U1352B based on the precruise time/depth function, Brusova (2010) and synthetic seismogram compared to depths of correlative lithologic surfaces observed sequence boundaries in cores.

Sequence Boundary	TWT (s) BSF	Precruise function depth (m)	Brusova function depth (m)	Synthetic depth (m)	Observed sequence boundary from core (m)
U1352B-19	0.087	68.4	68.6	73.7	62.15
U1352B-18	0.175	142.4	141.4	150	147.22
U1352B-17	0.234	194.8	192.46	196.8	207.04
U1352B-16	0.292	248.5	244.6	245	246.59
U1352B-15	0.472	428.6	420.1	403.4	423.84
U1352B-14	0.491	448.8	440	419.5	453.12
U1352B-13	0.539	500.8	491.7		
U1352B-11	0.77	771.9	772.5		
U1352B-9	0.924	971.3	998.5		
U1352B-8	1.043	1135.8	1201.6		
U1352B-7	1.124	1252.9	1356.7		
U1352B-6	1.241	1429.3	1606.2		

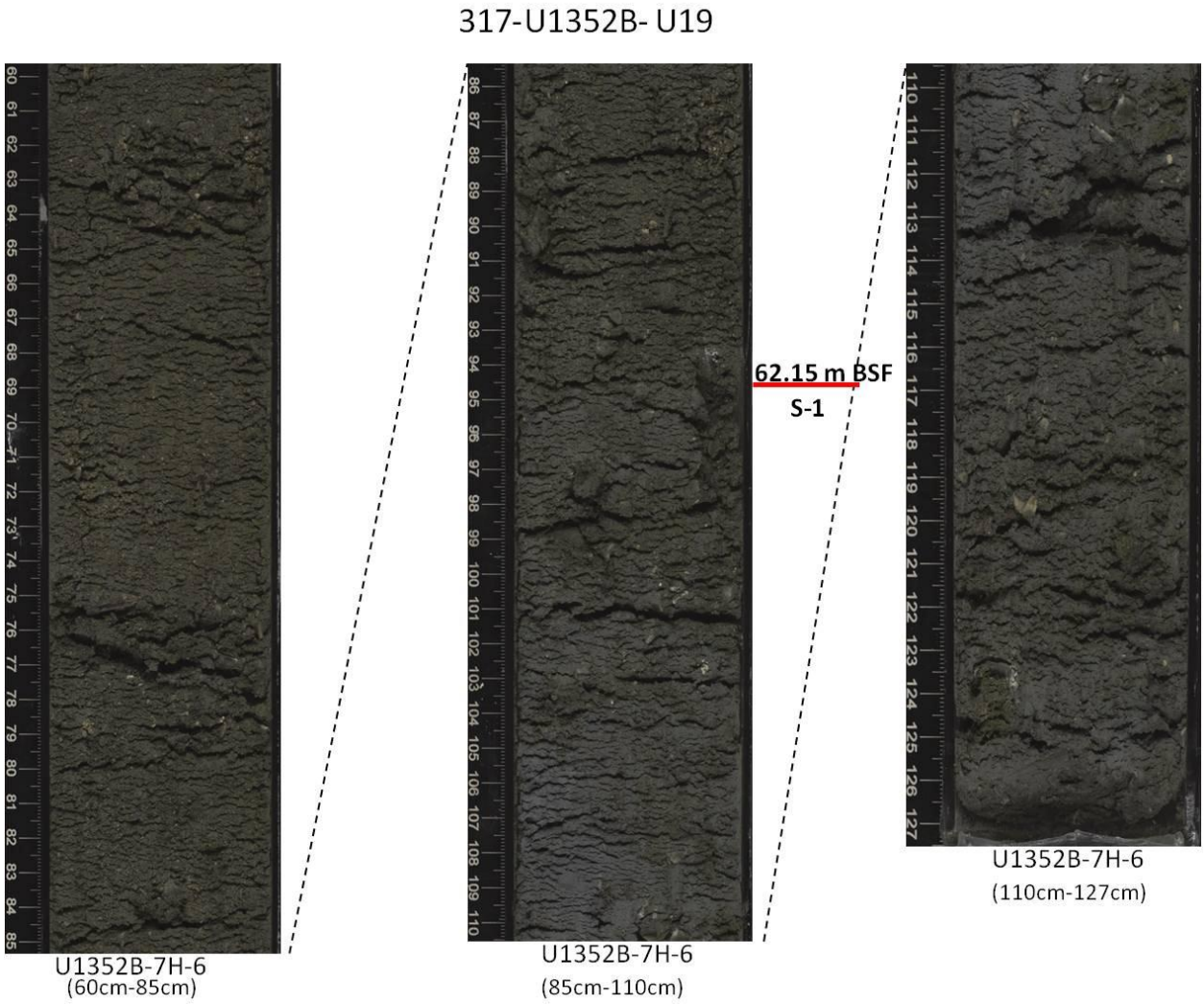

Figure 4.10: Core section U1352B-7H-6 showing lithologic boundary U1352B-S1 as a sharp basal contact at 62.15 m separating thick dark greenish gray fine to medium calcareous sand with scattered shell fragments from underlying dark greenish gray shelly mud with infilled centimeter-diameter burrows. This surface is correlated with the seismic sequence boundary U19.

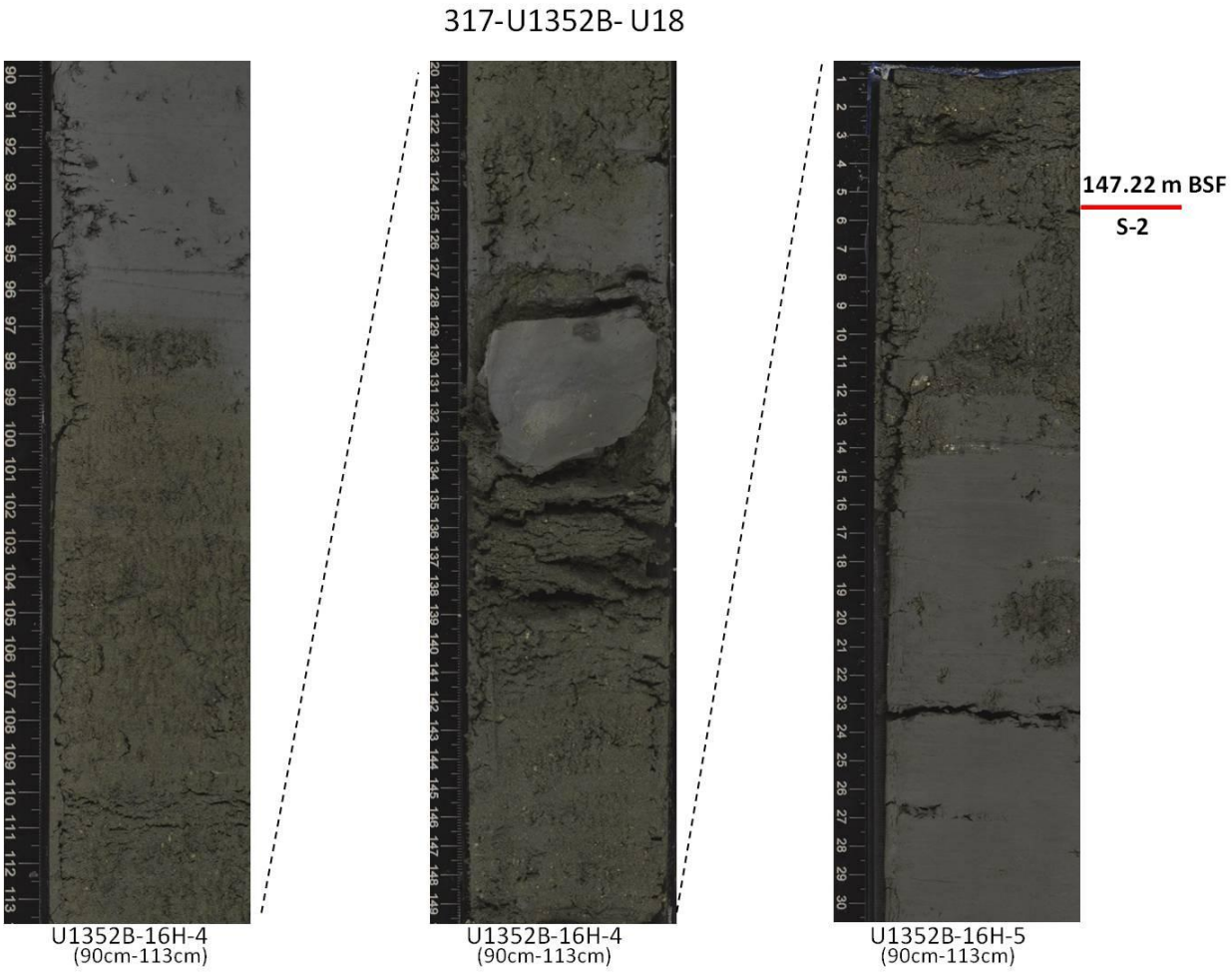

Figure 4.11: Core sections U1352B-16H-4 and U1352B-16H-5 showing lithologic boundary U1352B-S2. A heavily burrowed sharp basal contact at 147.22 m separates greenish gray muddy calcareous sand with scattered shell fragments from underlying dark gray to greenish gray mud. This contact is correlated with the seismic sequence boundary U18.

Figure 4.12: Core sectionU1352B-23H-6 showing lithologic boundary U1352B-S3, a heavily burrowed sharp basal contact at 207.04 m separating dark greenish muddy sand beds with rare shell fragments from underlying gray mud burrowed sand extend up to 23 cm. This contact is correlated with the seismic sequence boundary U17.

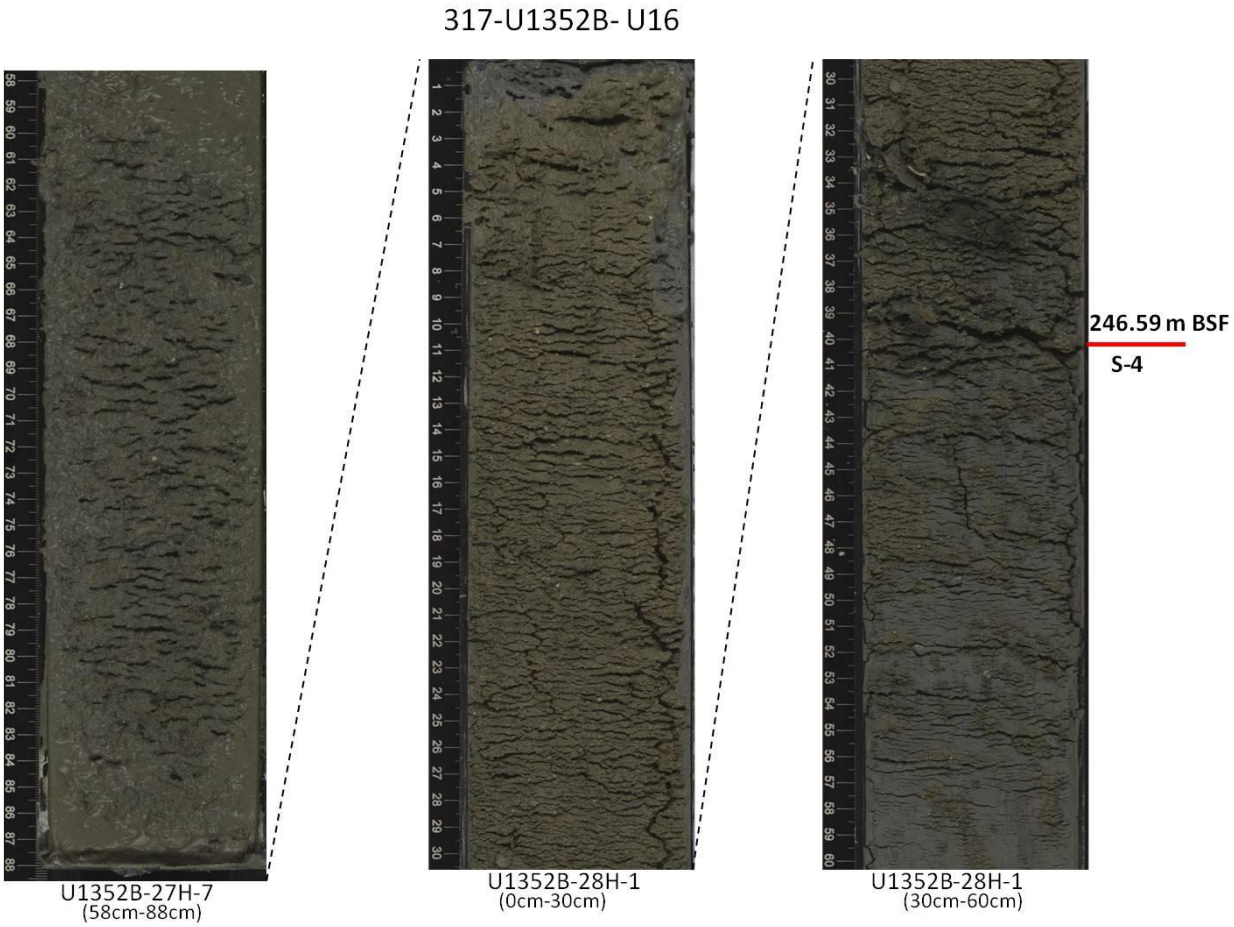

Figure 4.13: Core sections U1352B-27H-7 and U1352B-28H-1 showing lithologic boundary U1352B-S4, a heavily burrowed sharp basal contact at 207.04 m separating bioturbated dark greenish muddy sand from underlying burrowed gray mud. This contact is correlated with the seismic sequence boundary U16.

U1352B-S5: This boundary is a sharp contact and separates overlying thick 40 cm dark greenish gray fine to medium calcareous sand from underlying dark greenish gray sandy mud and gray mud. The contact is identified at depth of 423.67 m below sea floor in section 317-U1352B-50X-4, at 127 cm (Figure 4.14). This contact is ~5 m shallower from tentative shipboard placement in core because it is clearer and gradational lithologic transitions are increasing with depth. Concentrations of shell fragments are rare. This contact is observed near the predicted depth of seismically interpreted sequence boundary U15 and is correlated with that boundary. The closest depth prediction for U15 was provided by the Brusova (2010) function, which placed U15 ~4 m shallower than U1352-S5 (Table 4.2).

U1352B-S6: This is the deepest lithologic surface and inferred sequence boundary observed at site U1352B, because of the increasingly gradational lithologic transitions with depth, coupled with decreasing core recovery. The boundary is located at 453.12 m below sea floor in section 317-U1352B-53X-5, at 42 cm, where the heavily burrowed contact separates a thick overlying (>6 m) layer of very fine to fine greenish gray calcareous sand with rare scattered shell fragments, from underlying homogeneous mud (Figure 4.15). This contact is observed near the predicted depth of seismic sequence boundary U14. The precruise function yields the best depth correlations between core and seismic, placing ~4.5 m shallower than U1352B-S6 (Table 4.2). In addition, previous tentative shipboard placement of the boundary in core is ~ 30 m deeper from our observation, but it is considerably far from the predicted depth of seismic sequence boundary U14 (Table 4.2).

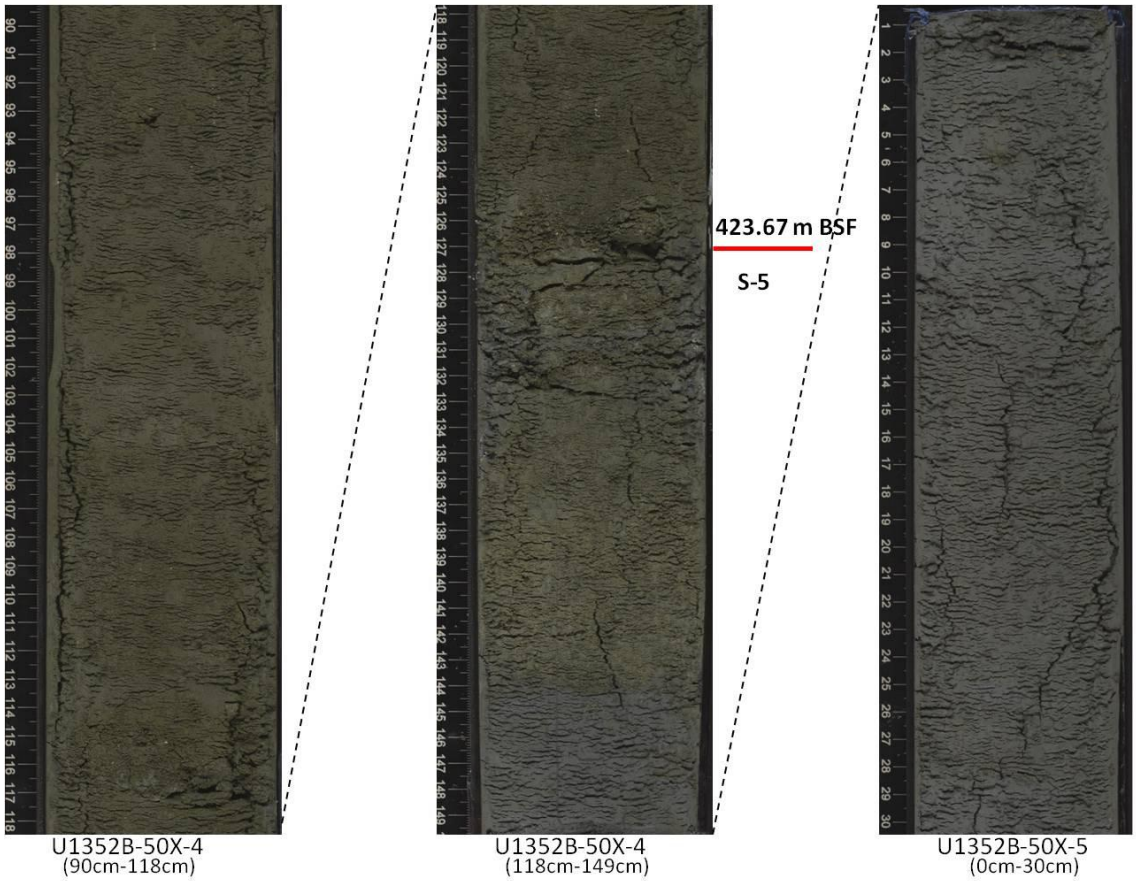

Figure 4.14: Core sections U1352B-50X-4 and U1352B-50X-5 showing lithologic boundary U1352B-S5, a sharp basal contact at 423.67 m separating dark greenish gray fine to medium calcareous sand from underlying dark greenish gray sandy mud and gray mud. This contact is correlated with the seismic sequence boundary U15.

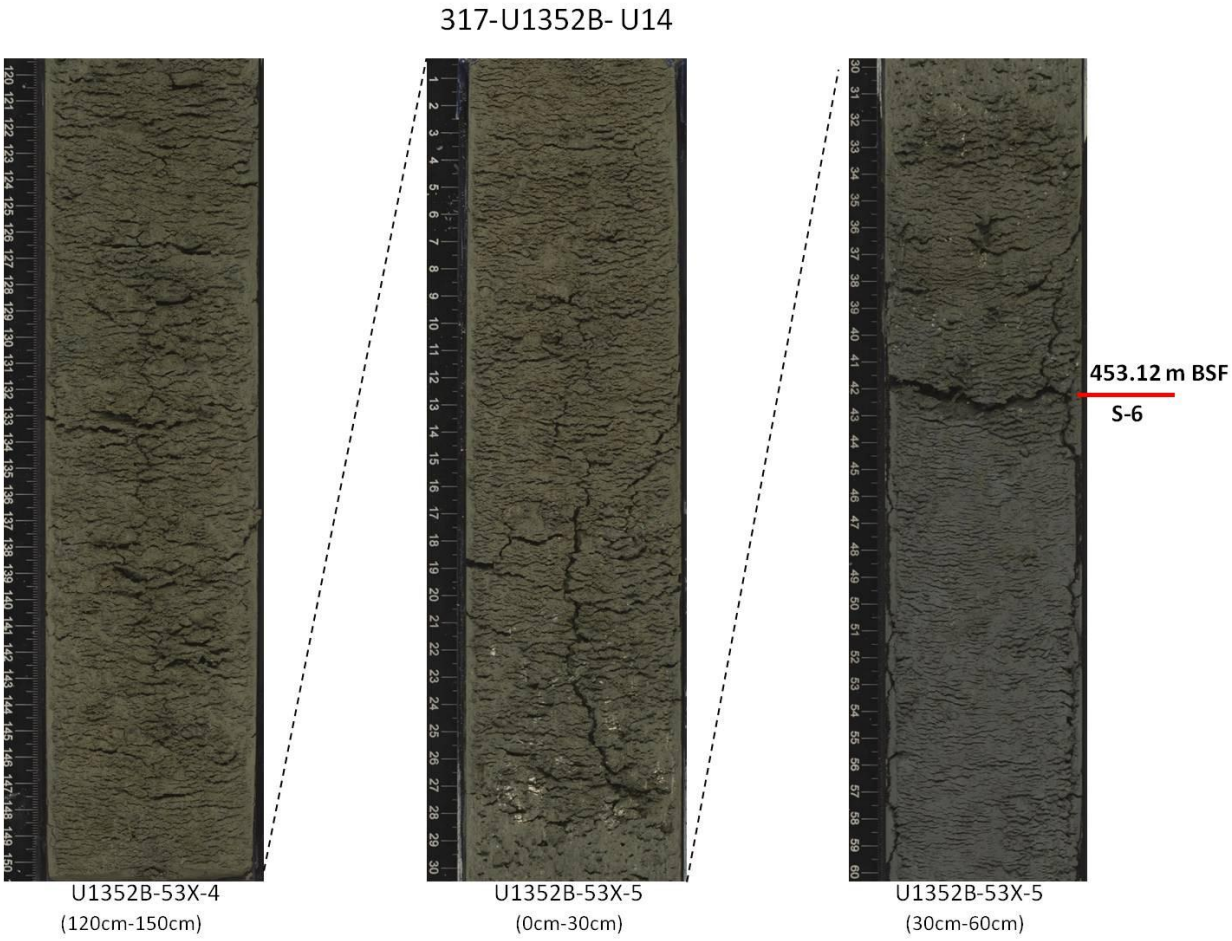

Figure 4.15: Core section U1352B-53X-4 and U1352B-53X-5 showing lithologic boundary U1352B-S6, a heavily burrowed sharp basal contact at 453.12 m separating very fine to fine greenish gray calcareous sand with rare scattered shell fragments from underlying homogeneous mud. This contact is correlated with the seismic sequence boundary U14.

CHAPTER 5: SUMMARY AND CONCLUSIONS

5.1 INFLUENCE OF CURRENTS ON DEPOSITION

Both seismic and core data show that current activity is a prominent process responsible for the Neogene sedimentary architecture of the offshore Canterbury Basin. Current controlled sedimentation resulted in both elongate and plastered sediment drifts together with sediment waves on paleoslopes. The role of currents was originally recognized by Fulthorpe and Carter (1991). Subsequently, Lu et al. (2003) and Lu and Fulthorpe (2004) interpreted 11 large elongate drifts within the early Miocene to Recent section (Figure 3.1). Drift deposition began in, the southwestern part of the study area and migrated northeastward, with the drifts increasing in height as aggradation of the shelf/slope system created increasing accommodation space basinward of the shelf edge.

One of the youngest and largest drifts, D10, is up to 1000 m thick and 20 km wide in the dip direction (Figure 3.1). It was initiated at around U6 time, probably, slightly earlier (Figure 5.1). D10 can be traced from northeast to southwest across the seismic grid but Lu and Fulthorpe (2004) did not recognize any extension D10 on southwestern dip profiles in the vicinity of the Expedition 317 sites (Lu and Fulthorpe, 2004; see their Figure 13). However, I have identified two previously unrecognized plastered drifts D10.1 and D10.2 on profiles in the southwestern part of the survey area (Figures 3.1, 3.3 and 3.4). These late Miocene plastered drifts are bounded below by seismic sequence boundary U-6 (10.4 Ma) and above by seismic sequence boundary U-7 (9 Ma), making them coeval with D10. The seismic signature of these plastered drifts includes (1) low-relief accumulation in a paleo-slope setting; (2) convex-upward mounded geometries;

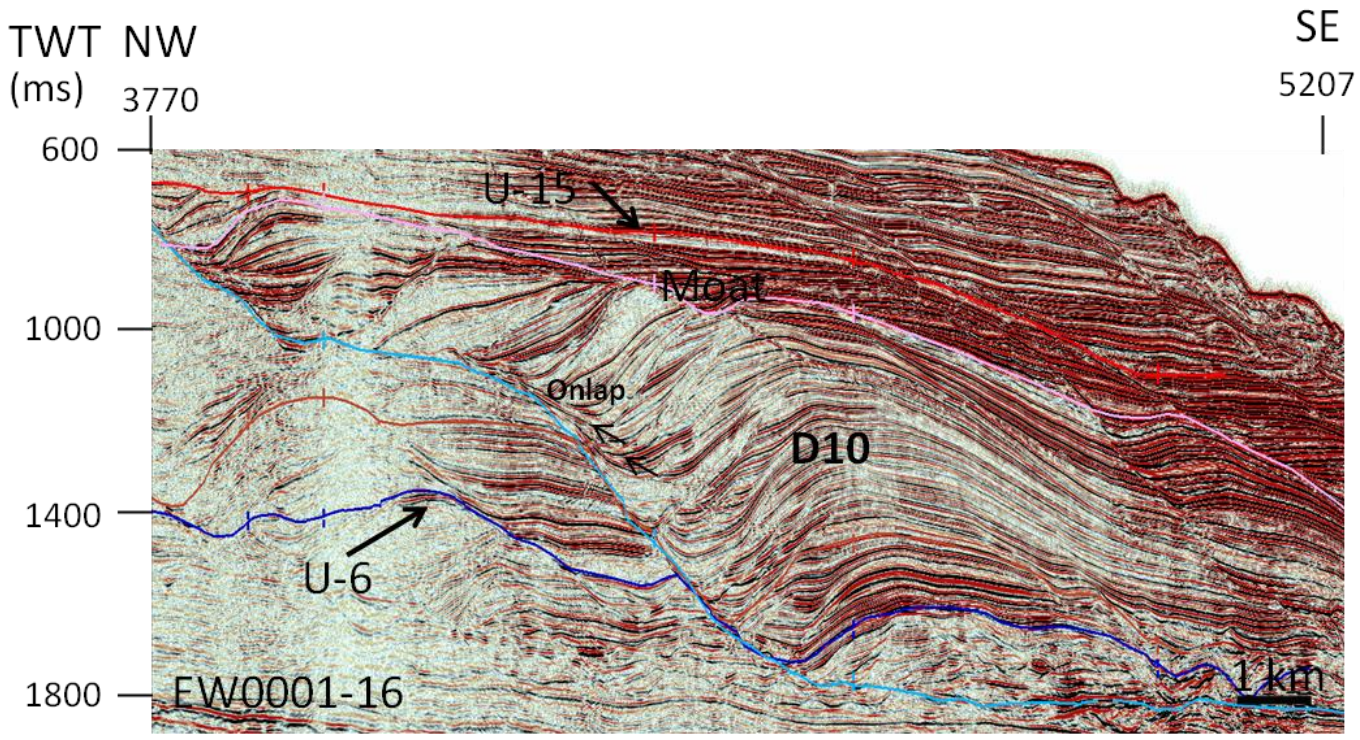

Figure 5.1: Seismic profile EW00-01-16 showing late simple elongate drift D10 with well-developed moat landward of the drift mound. D10 lies mostly between late Miocene sequence boundary U-6 and Pliocene sequence boundary U-15. The top and bottom of the drift are shown by pink and light blue lines, respectively. Vertical axis in two-way travel time. See Figure 3.1 for location.

(3) continuous flat-lying, discontinuous and wavy reflections within the drift; (4) internal reflections that onlap landward and downlap basinward. Plastered drifts D10.1 and 10.2 may be thought of either as distal, southwesterly extensions of elongate drift D10. Alternatively, drifts D10.1 and D10.2 may have formed entirely separately from D10. In that case, their small scale relative to D10 must be a result of differing sediment transport and depositional regimes operating in the southwestern part of the survey area relative to that in the northeast. Changes in paleobathymetry and seafloor morphology associated with progradation of the shelf/slope system, possibly in association with changes in sediment influx to the basin (Stagpoole, 2002; Sutherland & Browne, 2003), shifted the locus of elongate drift deposition to the northwest (Lu et al., 2003; Lu and Fulthorpe, 2004). However, we now recognize that drift deposition did not cease entirely in the southwest, but continued in a more subdued form with the deposition of plastered drifts in contrast to the larger elongate drifts that developed to the northwest.

Channel incisions on the top of the drift D10.2 (Figure 3.4) and coeval clinoform formation upslope and above drift D10.2 between sequence boundaries U6 and U7 (Figure 3.4) indicate that current activity was not only sedimentary processes action on the paleoslope after the early-mid Miocene. Drifts focus deposition on the paleoslope and therefore tend to reduce slope inclination (Lu and Fulthorpe, 2004). Therefore, as the locus of elongate drift deposition moved northeastward, paleoslope inclination increased in the southwest. This increase in slope inclination favored downslope sediment transport, which has interacted with along-strike processes. This is reflected in Expedition 317 cores from the southwestern part of the survey area, which are interpreted to contain evidence of both downslope and along-strike processes (Fulthorpe et al., 2011). In contrast, cores from ODP Site 1119 to the northeast were interpreted as reflecting entirely along-strike sediment transport and deposition (Shipboard Scientific

party, 1999; Carter et al., 2004). Seismic evidence of a sediment wave field on mid- and lower paleoslopes near the Expedition 317 sites (Figure 3.5), coupled with core evidence of sediment traction (Figure 3.6) indicate that current processes were still important contributors to deposition in the southwestern survey area into the late Pliocene-early Pleistocene (~U13-U16 time). The sediment waves are represented by alternating low to high amplitude reflections trend and climbing sinusoidal geometries through their upslope flanks. Cores through the sediment waves from Site U1352 provide information about the principal facies forming the sediment waves. The general facies are fine-grained mud rich sediment interbedded decimeter-centimeter thick sand and sandy mud. The distinct properties of sediment waves in core include (1) poorly developed sedimentary structures or structureless; (2) sharp upper and lower contacts; (3) occasional rhythmic centimeter- to decimeter-scale sand and mud layers. Expedition 317 scientists inferred from the cores that downslope processes were becoming dominant by this U13-U16 time (Fulthorpe et al., 2011). The increasing dominance of downslope sediment transport accompanied after the increase in eustatic amplitudes since the late Pliocene (~1.8 Ma) (Lu and Fulthorpe, 2004). This transition resulted in increasingly chaotic and high-amplitude seismic reflections on the upper slope (Figures 3.5 and 4.2) and beneath the shelf (Figure 4.1) as downslope transport became increasingly dominant between U13-U16 time. However, sediment waves on the middle to lower slope and at slope toes indicate that current activity could influence sediment deposition in those settings (Figures 3.5 and 4.2). The sharp basal contacts below sand layers at lithologic boundaries S4 and S5, which correlate with sequence boundaries U16 and U15, respectively, are similar to the evidence for current activity presented in Figure 3.6 and could also be products of current erosion (Figures 4.13 and 4.14). If current intensity increased during eustatic falls, currents may have played a role in sequence boundary formation.

5.2 CORE SEISMIC CORRELATION

Lithologic discontinuity surfaces and transitions together with associated sediment packages form the basis for identifying sequence boundaries in the cores. Contacts and facies were defined using shipboard core descriptions, emphasizing grain-size contrasts and the natures of the lower and upper contacts of sediment packages. Lithologic boundaries correlative with seismic sequence boundaries are identified and labeled in cores from lithostratigraphic Unit 1 at shelf Site U1351 (surfaces S1-S7) and slope Site U1352 (surfaces S1-S6). In this study, surfaces S2, S4, and S5 at shelf Site U1351 and surfaces S4, S5 and S6 at slope Site U1352 are placed at different locations in the cores, from their tentative placement by shipboard scientist during Expedition 317. The limited depths achieved by downhole logging, in particular sonic and density logs, together with poor recovery and increasingly gradational lithological contacts in the deeper section (lithostratigraphic Unit 2), did not allow investigation of older lithologic surfaces and their correlation with seismic sequence boundaries. Lithologic surfaces S1-S7 at shelf Site U1351 and S1-S6 at slope Site U1352 are correlated with early Pleistocene to recent seismic sequence boundaries U12-U19 and U14-U19, respectively. Three different traveltime/depth conversion methods were evaluated to calibrate core-seismic correlations: 1) a pre-Expedition 317 time/depth function (precruise function) developed primarily from well logs from the Clipper-1 exploration well, 2) a time/depth function developed by Brusova (2010) based on compaction characteristics and porosity trends together with lithologic information for sand, silt and clay from Clipper-1 and Expedition 317 sites, and 3) synthetic seismograms derived from Expedition 317 sonic and density logs from Sites U1351 and U1352. The result of this comparison is that no single approach provides an optimal time/depth conversion for all depth ranges. The time/depth

curve derived from the synthetic yields lower depths than the other methods over most depth ranges and works well within 5 m accuracy for the mid- to late Pleistocene.

REFERENCES

Bacon, M., Simm, R., & Redshaw, T., 2003. 3-D seismic interpretation. Cambridge, U.K: Cambridge University Press.

Balance, P.F., 1993. The paleo-Pacific, post-subduction, passive margin thermal relaxation sequence (Late Cretaceous to Paleogene) of the drifting New Zealand continent. In:Balance, P.F.(Ed) South Pacific Sedimentary Basins, Sedimentary Basins of the World 2, Elsevier: 93-110.

Bradshaw, J.D., 1989. Cretaceous geotectonic patterns in the New Zealand Region. Tectonics, Vol. 8, No. 4, p.803-820.

Brusova, O., 2011. Compaction of deep sea siliciclastic sediments based on log data.

Carter, R. T., & Norris, R. J., 1976. Cainozoic history of southern New Zealand: an accord between geological observations and plate-tectonic predictions. *Earth and planetary science letters*, *31*(1), 85-94.

Carter, R.M., 1988. Plate boundary tectonics, global sea-level changes and the development of the eastern South Island continental margin, New Zealand, Southwest Pacific. *Plateau*, *5*.

Carter, L., & McCave., I.N., 1994. Development of sediment drifts approaching an active plate margin under the SW Pasific Deep Western Boundary Undercurrent. *Paleoceanography* 9 (6), 1061-1085.

Carter, R.M., Fulthorpe, C.S., & Naish, T.R., 1998. Sequence concepts at seismic and outcrop scale: the distinction physical and conceptual stratigraphic surfaces: Sedimentary Geology, v. 122, p. 165-179.

Carter, L., Carter, R M, & Mccave, I. N., 2004. Evolution of the sedimentary system beneath the deep Pacific inflow off eastern New Zealand. *Sites The Journal Of 20Th Century Contemporary French Studies*, *205*. doi: 10.1016/S0025-3227(04)00016-7.

Carter, R.M., Gammon, P.R., and Millwood, L., 2004, Glacial-interglacial (MIS 1-10) migrations of the Subtropical Front across ODP Site 1119, Canterbury Bight, Southwest Pacific Ocean, *Marine Geology*, 205, p. 25-58.

Cox, S. C., & Sutherland, R., 2007. Regional Geological Framework of South Island , New Zealand , and its Significance for Understanding the Active Plate Boundary. *North*.

Ediger, V., Velegrakis, A. F., & Evans, G., 2002. Upper slope sediment waves in the Cilician Basin, northeastern Mediterranean. *Marine geology*, *192*(1), 321-333.

Einken, O., & Hinz, K., 1993. Sedimentary characteristics of Late Pleistocene bottom current deposits, Barets Sea slope off northern Norway. Sediment. Geol 82 (1-4), 15-32.

Expedition 317 Scientists, 2011. Expedition 317 summary. *In* Fulthorpe, C.S., Hoyanagi, K., Blum, P., and the Expedition 317 Scientists, *Proc. IODP,* 317: Tokyo (Integrated Ocean Drilling Program Management International, Inc.). doi:10.2204/iodp.proc.317.101.2011.

Faugères, J.C., Stow, D. A. V., Imbert, P., Viana, A. R., & Wynn, R. B., 1999. Seismic features diagnostic of contourite drifts. *Marine Geology*, 162, 1-38.

Faugères J-C, Stow D.A.V., 2008. Contourite drifts: nature, evolution and controls. In: Rebesco M, Camerlenghi A (Eds). Developments in sedimentology, vol 60. Elsevier, Amsterdam, pp 259–288.

Fulthorpe, C.S, & Carter, R M., 1989. Test of seismic sequence methodology on a Southern Hemisphere passive margin : the Canterbury Basin , New Zealand. *Test*, *6*.

Fulthorpe, C.S, & Carter, R.M., 1991. Geological Society of America Bulletin Continental-shelf progradation by sediment-drift accretion. *Geological Society Of America Bulletin*, (2). doi: 10.1130/0016-7606(1991)103<0300.

Fulthorpe, C.S., Carter, R.M., Miller, K. G., & Wilson, J., 1996. Marshall Paraconformity : a mid-Oligocene record of inception of the Antarctic Circumpolar Current and coeval glacio-eustatic lowstand. *Science*, *13*(1), 61-77.

Haq, B.U., Hardenbol, J., & Vail, P.R., 1987. Chronology of fluctuating sea levels since the Triassic. *Science,* 235(4793):1156–1167. doi:10.1126/science.235.4793.1156.

Hawkes, P.W., & Mound, D.G., 1984. Clipper-1 geological completion report. *N. Z. Geol. Surv. Open-File Rep.,* 1036.

Heat, R.A., 1972. The southland current, New Zealand Journal of Marine and Freshwater Research, 6:4, 497-533.

Heat, R.A., 1981. Oceanic fronts around southern New Zealand. Deep-Sea Research 28A: 547-560.

Howe, J. A., Stoker, M. S., & Stow, D.A.V., 1994. Late Cenozoic sediment drift complex, NE Rockhall Trough, North Atlantic. *Palaeoceanography,* 9, 989-999.

Kamp, P. J. J., 1986a. Geological Society of America Bulletin The mid-Cenozoic Challenger Rift System of western New Zealand and its implications for the age of Alpine fault inception. *Geological Society Of America Bulletin*. doi: 10.1130/0016-7606(1986)97<255.

Kamp, P. J. J., 1986b. The Australia , Antarctica and Pacific plates interact in the southwest Pacific ' SF. *Science*, *121*, 225-251.

King, P R., 2000. New Zealand ' s changing configuration in the last 100 million years : plate tectonics , basin development , and depositional setting. *Sciences-New York*, (March).

Laird, M. G., & Bradshaw, J. D., 2004. The Break-up of a Long-term Relationship : the Cretaceous Separation of New Zealand from Gondwana. *Offshore (Conroe, TX)*, (I).

Lu, H., & Fulthorpe, C.S., 2004. Controls on sequence stratigraphy of a middle Miocene – Holocene , current-swept , passive margin : Offshore Canterbury Basin , New Zealand. *America*, (11), 1345-1366. doi: 10.1130/B2525401.1.

Lu, H., Fulthorpe, C.S, & Mann, P., 2003. Three-dimensional architecture of shelf-building sediment drifts in the offshore Canterbury Basin , New Zealand. *Marine Geology*, *193*.

Masson, D. G., Howe, J. A., & Stoker, M. S., 2002. Bottom-current sediment waves, sediment drifts and contourites in the northern Rockall Trough. *Marine Geology*, *192*(1), 215-237.

Mèzerais, M.L., Faugères, J.C., Figueiredo, A., & Massè, L., 1993. Contour current accumulation off Vema Channel mouth, southern Brazil basin. Sediment. Geol. 82 (1-4), 173-188.

McCave, I.N., Tucholke, B.E., 1986. Deep current-controlled sedimentation in the western North Atlantic. In: Vogt, P.R., Tucholke, B.E. (Eds.). The Geology of North America, Vol. M, The Western North Atlantic Region, Decade of North America Geology. Geol. Soc. Am., Boulder, CO, 451-468.

Molnar, P., Atwater, T., Mammerycx, J., and Smith, S.M., 1975. Magnetic anomalies, bathymetry and the tectonic evolution of the South Pacific since Later Cretaceous: Geophysical Journal of the Royal Astronomical Society, v. 40, p. 383-420.

Morris, M., Stanton, B., and Neil, H., 2001. Subantarctic oceanography around New Zealand: preliminary results from an ongoing survey. *N. Z. J. Mar. Freshwater Res.,* 35:499–519.

Norris, R J, & Zealand, N., 1990. The obliquely-convergent plate boundary in the South Island of New Zealand : implications for ancient collision zones, *12*(5).

Norris, Richard J, & Cooper, A. F., 2001. Late Quaternary slip rates and slip partitioning on the Alpine Fault , New Zealand. *Journal of Structural Geology*, *23* (2000).

Russell B.W., & Stow, D. A. V., 2002. Classification and characterization of deep-water sediment waves. *Environment*, *192*.

Shanmugam, G., Spalding, T. D., & Rofheart, D. H., 1993. Traction structures in deep-marine, bottom-current-reworked sands in the Pliocene and Pleistocene, Gulf of Mexico. *Geology*, *21*(10), 929-932.

Shipboard Scientific Party, 1999, Leg 181 summary: Southwest Pacific paleoceanography. *In* Carter, R.M., McCave, I.N., Richter, C., Carter, L., et al., *Proc. ODP Init. Repts.*, 181, College Station, TX (Ocean Drilling Program), 1-80.

Stoker, M. S., Akhurst, M. C., Howe, J. A., & Stow, D. A. V. 1998. Sediment drifts and contourites on the continental margin off northwest Britain. *Sedimentary Geology*, *115*(1), 33-51.

Stow, D. A. V., Faugères, J.C., Howe, J. A., Pudsey, C. J., & Viana, A. R., 2002. Bottom currents , contourites and deep-sea sediment drifts : current state-of-the-art. *Society*, 6-20. doi: 10.1144/GSL.MEM.2002.022.01.02.

Taylor, P., King, P.R., 2010. New Zealand Journal of Geology and Geophysics Tectonic reconstructions of New Zealand : 40 Ma to the Present Tectonic reconstructions of New Zealand : 40 Ma to the Present. *Society*, (April 2012), 37-41.

Wood, R. A., & Stagpoole, V. M., 2007. Validation of tectonic reconstructions by crustal volume balance : New Zealand Validation of tectonic reconstructions by crustal volume balance : New Zealand through the Cenozoic. *Geological Society of America Bulletin*. doi: 10.1130/B26018.1.

Wilding, A., and Sweetman, I.A.D., 1971. Endeavour-1 petroleum report. *N. Z. Geol. Surv. Open-File Rep.,* 303.

Wilson, I.R., 1985. Galleon-1 geological completion report. *N. Z. Geol. Surv. Open-File Rep.,* 1146.